Multiscale Anisotropic Tissue Biofabrication via Bulk Acoustic Patterning of Cells and Functional Additives in Hybrid Bioinks

Parth Chansoria^{1,2}, Suleman Asif^{1,2}, Nithin Gupta^{2,3}, Jorge Piedrahita^{2,3}, Rohan A. Shirwaiker^{1,2,4,5}*

P. Chansoria, S. Asif

Edward P. Fitts Department of Industrial and Systems Engineering, and Comparative Medicine Institute, North Carolina State University, Raleigh, NC 27695, USA

N. Gupta, J. Piedrahita

Department of Molecular Biomedical Sciences, and Comparative Medicine Institute, North Carolina State University, Raleigh, NC 27695, USA

R. A. Shirwaiker

Edward P. Fitts Department of Industrial and Systems Engineering, Comparative Medicine Institute, Joint Department of Biomedical Engineering, and Department of Mechanical and Aerospace Engineering, North Carolina State University, Raleigh, NC 27695, USA

Email: rashirwaiker@ncsu.edu

Keywords: ultrasound, biofabrication, bioprinting, standing bulk acoustic wave, 3D cell patterning, GelMA, hybrid bioinks

Recapitulation of the microstructural organization of cellular and extracellular components found in natural tissues is an important but challenging feat for tissue engineering, which demands innovation across both process and material fronts. In this work, we demonstrate a highly versatile ultrasound-assisted biofabrication (UAB) approach that utilizes radiation forces generated by superimposing ultrasonic bulk acoustic waves to rapidly organize arrays of cells and other biomaterial additives within single and multi-layered hydrogel constructs. We use UAB in conjunction with a novel hybrid bioink system, comprising of cartilage-forming cells (human adipose-derived stem cells or chondrocytes) and additives to promote cell adhesion (collagen microaggregates or polycaprolactone microfibers) encapsulated within gelatin methacryloyl

(GelMA) hydrogels, to fabricate cartilaginous tissue constructs featuring bulk anisotropy. The hybrid matrices fabricated under the appropriate synergistic thermo-reversible and photocrosslinking conditions demonstrate enhanced mechanical stiffness, stretchability, strength, construct shape fidelity and aligned encapsulated cell morphology and collagen II secretion in long-term culture. We also show hybridization of UAB with extrusion and stereolithography printing to fabricate constructs featuring 3D perfusable channels for vasculature combined with a crisscross or circumferential organization of cells and adhesive bioadditives, which is relevant for further translation of UAB towards complex physiological-scale biomimetic tissue fabrication.

1. Introduction

Central to the function of most tissues in the human body is the specific organization of the constitutive cells and extracellular matrix (ECM) components. As an example, the connective tissue fibers in the epicardium are inclined at 70° to the circumference of the heart (longitudinal direction)^[1,2]. As a result, the epicardium is stiffer and undergoes less deformation in the transverse direction (0.2-0.5 MPa modulus^[3], 2-6% strain^[4]) compared to the longitudinal (0.05-0.25 MPa modulus^[5], 3-10% strain^[4]). Not only is the anisotropy in these tissues directionally dependent, but the predominant orientation and composition of the biological components also varies significantly across different regions of the tissue. For example, the knee meniscus features a predominantly circumferential organization of the constitutive fibrochondrocytes and collagen fibers with interspersed radial tie-fibers to further enhance the load bearing capability of the tissue^[6]. A similar orientation of the cells and cell-secreted ECM fibers is also evident in the collagen fibers of the lung^[7,8], smooth muscle in the stomach and the colon^[9], and the muscle and tendon of the diaphragm^[6].

For tissue engineering strategies aiming to create biomimetic tissues, achieving the appropriate organization of cells is a precursor to achieving the desired organization of ECM and biomechanical functionality. Studies using fibrous polymer scaffolds, such as those made using electrospinning^[10], melt-blowing^[11] and extrusion printing^[12] have typically relied on microarchitectural contact guidance to impart cell and ECM organization along the fiber orientation. Of late, bioprinting of cell-laden bioinks has been established as a versatile technology for fabrication of complex tissues such as the heart^[13,14], liver^[15,16] and skin^[17,18], featuring multiple types of cells, biomaterial matrices and additives. Since the homogeneous distribution of cells within bioinks can be a limiting factor in achieving the anisotropic ECM organization, researchers

have investigated cellular organization within bioinks using electrical^[19,20], optical^[21,22], magnetic^[23,24] or acoustic^[25,26] tweezing, and chemotactic^[27,28] modalities. Among these, acoustic tweezing (also known as acoustophoresis) has gained substantial interest in recent years as a highly versatile label-free^[29] and non-contact^[30] approach to rapidly organize cells within viscous hydrogel matrices. Some acoustophoretic approaches have utilized surface acoustic waves (SAW) for patterning cells relevant to anisotropic muscle^[31], nervous^[32] and vascularized^[33,34] tissue applications. As such, SAW-driven approaches require specialized substrate materials (e.g., lithium niobate) to enable the formation of standing acoustic waves, and the acoustic radiation forces generated are inadequate to achieve patterning of cells in viscous hydrogel constructs of physiologically-relevant thicknesses, thereby limiting effective integration with 3D bioprinting^[35]. In contrast, we focus on bulk acoustic wave (BAW)-driven manipulation of cells, which is independent of the bioink layer being printed (process mechanics described in the Supporting Information). We also use an open-top configuration of the ultrasonic patterning chamber (UPC), which allows easy integration with extrusion^[35,36] and vat photopolymerization^[37] printing, and which further distinguishes our work from previous BAW-based approaches^[38–40].

In their 3D microenvironment, encapsulated cells attach, elongate, proliferate, and mold the matrix around them to establish cell-cell contacts, which in-turn has been shown to be essential for increased ECM deposition^[31,41]. In tissue engineering, however, it is challenging to achieve an optimal matrix microenvironment for supporting cell growth and inter-cellular and cell-ECM interactions while maintaining structural fidelity of the 3D hydrogel matrix during long-term culture. To address this critical challenge, we present a new approach that leverages synergy between composite biomaterials and hybrid biofabrication to engineer tissue constructs with multiscale biomimetic cellular and extracellular organization and perfusable channels for vasculature. First, we first study the material-process-structure-function interactions to achieve a high degree of control over the patterning of cells in gelatin methacryloyl (GelMA) matrix via BAW-driven ultrasound-assisted biofabrication (UAB). The combinatorial thermo-reversible- and photogelation of GelMA^[42] are optimized to fabricate mechanically robust hydrogels that maintain shape fidelity during long-term culture^[43] while promoting cell proliferation. Then, we formulate GelMA composites featuring collagen-I microaggregates (CM) and polycaprolactone (PCL) microfibers (PM) that provide adhesion sites for cells and complement the RGD peptides in GelMA. These bioadditives not only improve the mechanical properties of the hydrogel, but when patterned alongside the cells, allow the adhered cells to align their morphology and produce ECM along the

patterned arrays, rendering biomimetic structural and mechanical anisotropy. Finally, to highlight scalability of this approach, we demonstrate hybridization of UAB with extrusion and stereolithographic printing to create multi-scale anisotropic and perfusable tissue constructs.

2. UAB Strategy for Fabricating Anisotropic Tissue Constructs

The scheme for UAB of anisotropic hydrogel constructs is illustrated in Figure 1A. The hydrogel bioink containing different combinations of cells and cell adhesion-promoting particles (CM/PM) is dispensed in the UPC consisting of a petri dish ($\emptyset = 35$ mm) with a piezo transducer opposite to a glass reflector. When the transducer is actuated at its resonant frequency (2 MHz in this study), the interference between the wave emanating from the transducer and the one reflected from the reflector generates a standing bulk acoustic wave (SBAW) in the bioink. This standing wave represents pressure variation in the bioink, with nodes along planes parallel to the walls of the transducer or the reflector and separated by half wavelength ($\lambda/2$). Acoustic radiation forces resulting from the SBAW act on the cells or particles that are not already at a pressure node to organize them along the nearest node, while the drag forces act to impede their motion. The analytical theory on the variation of pressure and the corresponding mechanics of cell/particle motion has been discussed in the Supporting Information. The estimated spatial distribution and magnitude of planar pressure nodes along which cells/particles can be expected to organize are highlighted in the results of the 3D computational model of the acoustic radiation pressure within the UPC (Figure 1B). At the top and bottom regions of the bioink (see cross-sectional view P2) the radiation pressure (and resulting cell/particle patterning) is negligible, since these regions experience acoustic damping due to a change in acoustic impedance at the bioink-air and bioink-UPC interfaces^[37]. After the cells/particles have organized within the matrix, the hydrogel is crosslinked. Herein, multiple crosslinking strategies are assessed. The bioink is either thermoreversibly crosslinked at 10°C or maintained at 37°C while being exposed to UV (405 nm) for different durations (6 and 10 s), and the non-photocrosslinked portions of GelMA are subsequently dissolved away by reheating to 37°C. The resultant constructs feature patterning of cells and the adhesive cues and a wide range of porosities and biomechanical properties within the GelMA matrices.

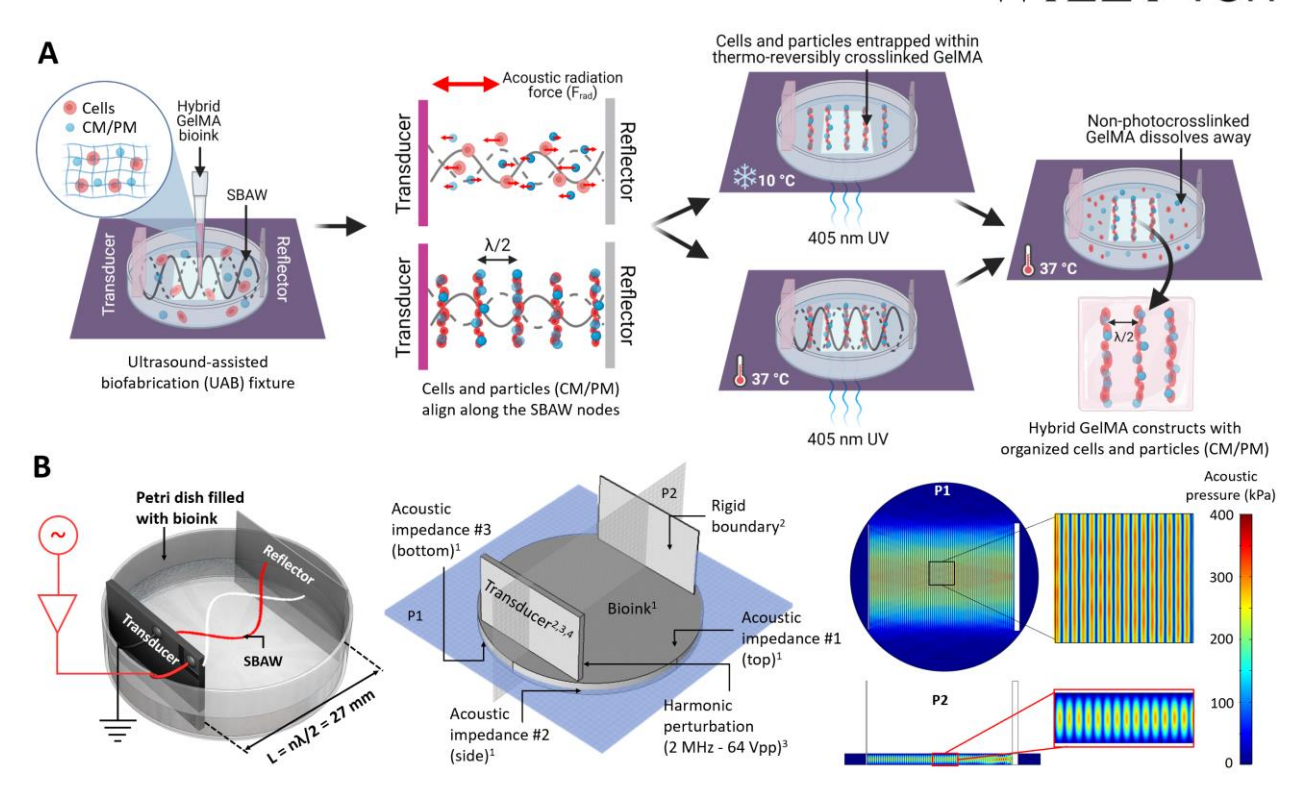


Figure 1. Ultrasound-assisted biofabrication and computational modeling. **A.** Scheme of fabrication of anisotropic hybrid hydrogel constructs featuring patterned cells and CM or PM. The hybrid GelMA bioink at 37°C is added to the UPC containing opposing transducer-reflector pairs. The actuation of the transducer at ultrasonic frequencies generates SBAW, which exerts radiation forces on the cells and particles, causing them to pattern along planes (3D patterning) parallel to the transducer/reflector surface. The bioink is then either thermos-reversibly crosslinked at 10°C prior to photocrosslinking, or directly photocrosslinked, causing the cells and particles to get entrapped in their patterned structures within the constructs. The constructs can then be extracted after removal of the non-photocrosslinked GelMA by reheating to 37°C. **B.** Setup for the 3D computational modeling of SBAW generation in UPC including the boundary conditions. The pressure distribution pattern (right) is along straight lines (max acoustic pressure amplitude is 400 kPa) as seen from the planar sections P1 (top view) and P2 (cross-sectional view), which is supportive of the analytical prediction that the cells and particles are patterned along parallel planes. The maximum acoustic radiation pressure amplitude is approximately 400 kPa along the antinodes of the SBAW.

3. Understanding Critical Material-Process-Structure-Function Interrelationships to Optimize UAB Process

Before the synthesis of functional tissue constructs, it is essential to understand the critical process-structure-function interrelationships, which relate to the effects of processing parameters on the functional properties of the matrix (matrix stability and porosity) and the bioadditives (CM/PM).

GelMA can undergo both thermo-reversible and photocrosslinking^[44], and the degree of each type of crosslinking can significantly affect the proliferation of encapsulated cells and matrix conformation during culture. CryoSEM images (**Figure 2A**) demonstrate the effects of thermo-reversible and photocrosslinking of GelMA on the hydrogel microstructure. Cooling GelMA below physiological temperatures induces entanglement of polypeptide networks, and subsequent UV crosslinking creates covalent bonds between the entangled networks to prevent their decrosslinking when the temperature is increased^[43], which is evident in the CryoSEM images (Figure 2A).

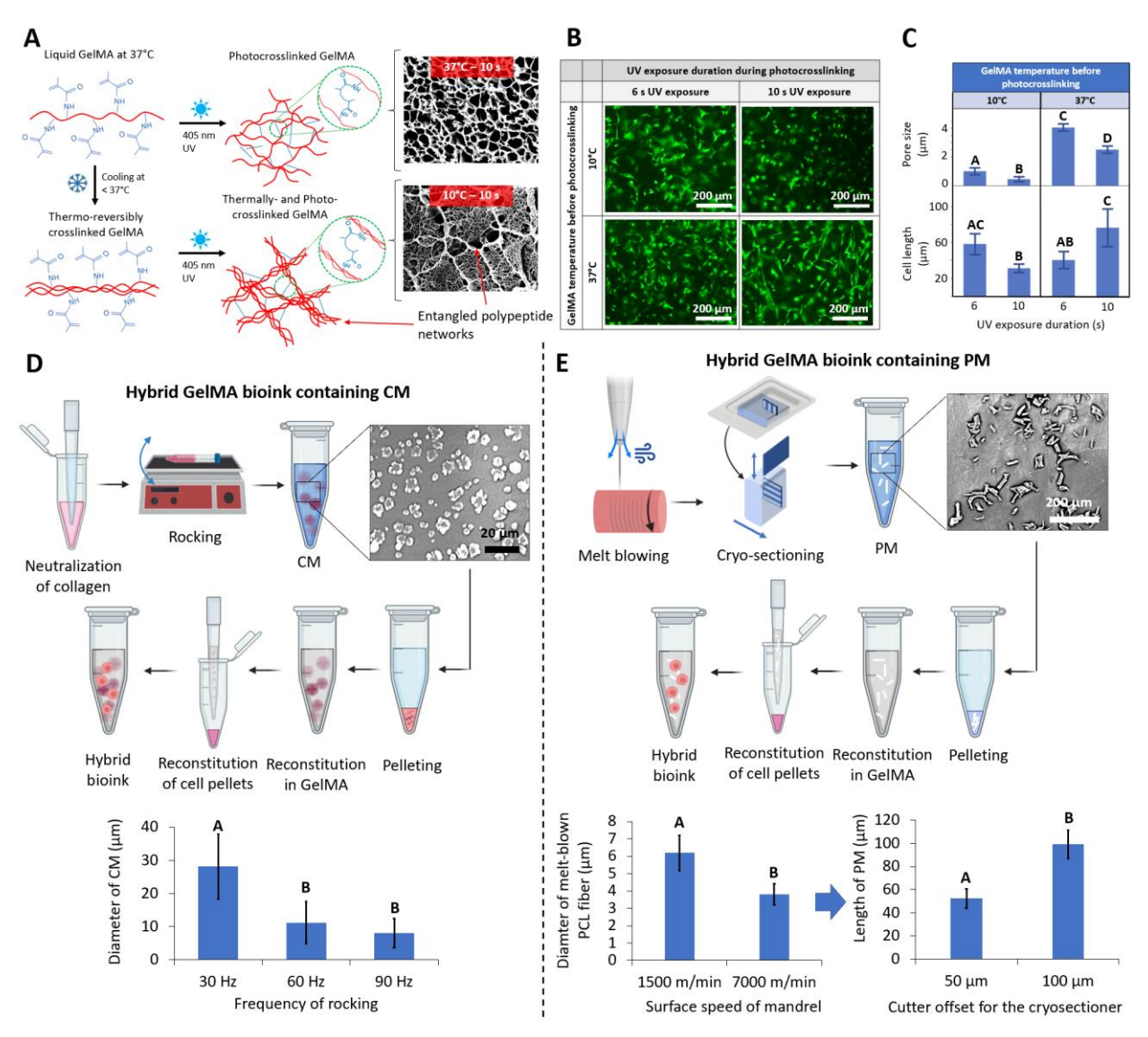


Figure 2. Investigating the effects of dual-crosslinking property of GelMA photoinks and synthesis of hybrid GelMA formulations containing CM or PM. **A.** Below 37°C, polypeptide chains of GelMA undergo tight interlinking leading to thermo-reversible gelation, and subsequent photocrosslinking leads to formation

of non-reversible covalent crosslinking of the GelMA matrix^[43]. Based on the pre-photocrosslinking solution temperature and subsequent UV exposure duration, varying degree of crosslinking can be achieved within the GelMA matrix. B. Live/dead staining of encapsulated cells, within the GelMA constructs made under varying temperature before crosslinking and subsequent photocrosslinking durations, after 3 days in culture. The viability was 100%, but the cell elongation was different in different groups. C. Analysis of pore size of the fabricated constructs determined via CryoSEM (procedure in methods section) and the length of the cell processes in the constructs after 3 days as determined via ImageJ. The 10°C-6 s and 37°C-10 s formulations lead to the highest cell elongation. **D.** Fabrication of CM via collagen crosslinking in the presence of media turbulence (induced by rocking the containing the neutralized collagen). Increase in the frequency of rocking leads to decrease in the size of the CM. E. Fabrication of PM via meltblowing[11] and subsequent cryosectioning. Increase in the surface speed of the collection mandrel leads to reduction in the diameter of melt blown PCL fibers, while increase in the cutter offset of the cryosectioner leads to increase in the length of the derived PM. The CM or PM can be centrifuged and suspended in GelMA to constitute the hybrid photoinks, and cells could later be added to constitute the hybrid bioinks. In each plot, letters A-D represent statistically significant differences (p < 0.05) determined from Tukey Posthoc HSD. Error bars denote standard deviation.

Figure 2B shows live/dead images of human adipose-derived stem cells (hASC) within GelMA hydrogels processed at different solution temperatures (10°C and 37°C prior to UV crosslinking) and UV exposure durations (6 and 10 s). After 3 days in culture, a 100% cell viability was observed in all four GelMA groups, which highlights the biocompatibility of the combinatorial crosslinking method. Figure 2C summarizes the corresponding hydrogel pore sizes determined via analysis of CryoSEM images using a custom MATLAB algorithm^[43] and the degree of cell elongation (i.e., length of the cell processes) determined via image analysis in the four GelMA groups. The pore sizes were found to impact cell elongation, although their relationship was nonlinear. The smallest pore size (0.51±0.11 µm) was observed in the 10°C-10 s group, resulting from the high degree of thermo-reversible interlinking of polypeptide chains induced by the initial lower solution temperature and a high density of covalent bond formation induced by the higher photocrosslinking duration, as hypothesized. The consistently smaller pores contributed to the lowest cell elongation (33.4±6.2 µm) in the design space. In contrast, the 37°C-6 s group was characterized by the largest pores (40.5±8.6 μm) but not the highest cell elongation. The 10°C-6 s group demonstrated similar cell elongation as the 37°C-6 s group despite possessing significantly smaller pores $(1.1\pm0.3 \mu m)$ (p < 0.05). This can be attributed to the presence of a few wider pores in between the small pores within the matrix, which accommodated some degree of cell elongation. The 37°C -10 s group, which had larger pores $(4.1\pm0.3~\mu\text{m})$ than the two groups processed at 37°C , featured the highest cell elongation $(78.3\pm20.1~\mu\text{m})$. These results highlight the relationship between hydrogel microstructure and cellular responses and signify the importance of using an optimal matrix density that promotes cell elongation, which can subsequently impact other cellular functional responses. Owing to the higher cell elongation within the matrix, the 10°C -6 s and 37°C -10 s formulations were selected for all subsequent studies in this work.

The new procedures for synthesizing the hybrid bioinks with the CM or PM additives are summarized in **Figure 2D** and **E**. Synthesis of CM involved neutralization of collagen in a medium while being subjected to constant turbulence via rocking. The turbulence resulted in shearing of the fibrils being formed during the crosslinking of the neutralized collagen, thereby resulting in CM. Depending on the shear rate of the collagen matrix, CM of different diameters could be formulated (Figure 2D). By increasing the rocking frequency from 30 to 90 Hz, the mean CM diameter reduced from 28.1 to 8.1 μ m, respectively (p < 0.05). For the fabrication of PM, melt blown fibrous PCL scaffolds^[11] were encapsulated in embedding solution, cryosectioned, and thoroughly washed. By controlling the melt blowing processing conditions and the length of the cryosections, a wide range of PM diameters and lengths were achieved (Figure 2E). Increasing the surface speed of the collection mandrel from 150 to 700 m/min during melt blowing resulted in a reduction of PCL fiber diameters from 6.2 to 3.8 μ m, respectively (p < 0.05). During subsequent cryosectioning, PCL fiber lengths of 52.3 and 99.1 μ m were achieved by increasing the cuter offset from 50 to 100 μ m, respectively (p < 0.05).

To study the patterning of cells and bioadditives in hybrid hydrogels via UAB, photoinks were constituted by centrifuging the CM (Ø11.2±6.4 μ m) or PM (Ø 6.2±1.4 μ m and length 52.3±8.2 μ m) and resuspending them in GelMA solution. The two hydrogel formulations that had demonstrated high cell elongation (10°C-6 s and 37°C-10 s groups) were investigated. Herein, **Figure 3A** plots represent the dynamics of the motion of the cells, CM and PM from the SBAW antinode to the nearest antinode during UAB. The derivation for different expressions (analytical theory section) has been provided in the Supporting Information. Within the UPC, nodes are formed in integer multiples of λ /2 nodes, with adjacent nodes separated by λ /2 and with an antinode in the middle. At the antinode (λ /4 = 187.5 μ m from the node in the present case), the acoustic radiation force (F_{radiation}) is negligible, since the cells/bioadditives are almost equally attracted to the nodes on either side. As the cells/particles start moving to the nearest node, the F_{radiation} increases and

reaches a maximum at the midpoint between the antinode and the node ($\lambda/8 = 93.75 \, \mu \text{m}$ from the node and the antinode in the present case, Figure 3A). For modeling purposes, the cells and CM are assumed to be governed by the physics of the motion of spherical particles^[36] within viscous fluids, while the PM are assumed to be cylindrical^[45]. Overall, the F_{radiation} is proportional to the size (length and/or diameter) and mass density of the particles (see Supporting Information). In the present case, F_{radiation} is the lowest for PM (Ø 6.2 µm and length 52.3 µm) and highest for hASC (Ø = $24 \mu m$). Importantly, the size does not necessarily correlate to the patterning time for the cells and additives. This is because the patterning time is based on the interplay between F_{radiation} causing cell/additives movement and drag forces (F_{drag}) opposing their movement, both of which are directly proportional to the cell/additive size. In the present case, the patterning of CM is the fastest, estimated to be < 100 s in continuous mode. The cells, which are twice the size of CM, pattern in approximately 170 s. The PM take the highest amount of time to pattern, estimated to be up to 200 s. Note that we use a burst mode of actuation during physical experiments, wherein the transducers are actuated for 1 s followed by a 1 s pause, to prevent deterioration of their acoustic properties due to overheating^[36]. Thus, the required patterning time would be at least twice the theoretical estimate^[36]. Accordingly, to ensure that the cells/additives were patterned prior to gelation, the GelMA solution was subject to the ultrasound for 5 min before commencing crosslinking.

After patterning (with or without thermo-reversible crosslinking), the constructs were irreversibly photocrosslinked via mask projection stereolithography into 1.5 mm thick dog-bone shaped hydrogels (**Figure 3B**). The resultant constructs featured patterning along and throughout their entire length, as is evident in the macro and microscopic images. They also featured consistent inter-array spacing of $\lambda/2 = 375 \, \mu m$, which corroborates the theory (Supporting Information).

Figure 3C summarizes the tensile properties of constructs, with and without CM or PM and with or without UAB-induced patterning, fabricated under the different thermo-reversible and photo-crosslinking conditions. Overall, the formulation condition (combination of temperature and UV exposure duration), presence of CM or PM, and UAB-induced patterning had a significant effect on the tensile properties of the constructs. Comparing the pure GelMA groups (without any additives), the 10°C-6 s formulation demonstrated significantly higher stiffness and tensile strength than the 37°C-10 s formulation, which can be attributed to the tighter interlinking of the constitutive polypeptide chains.

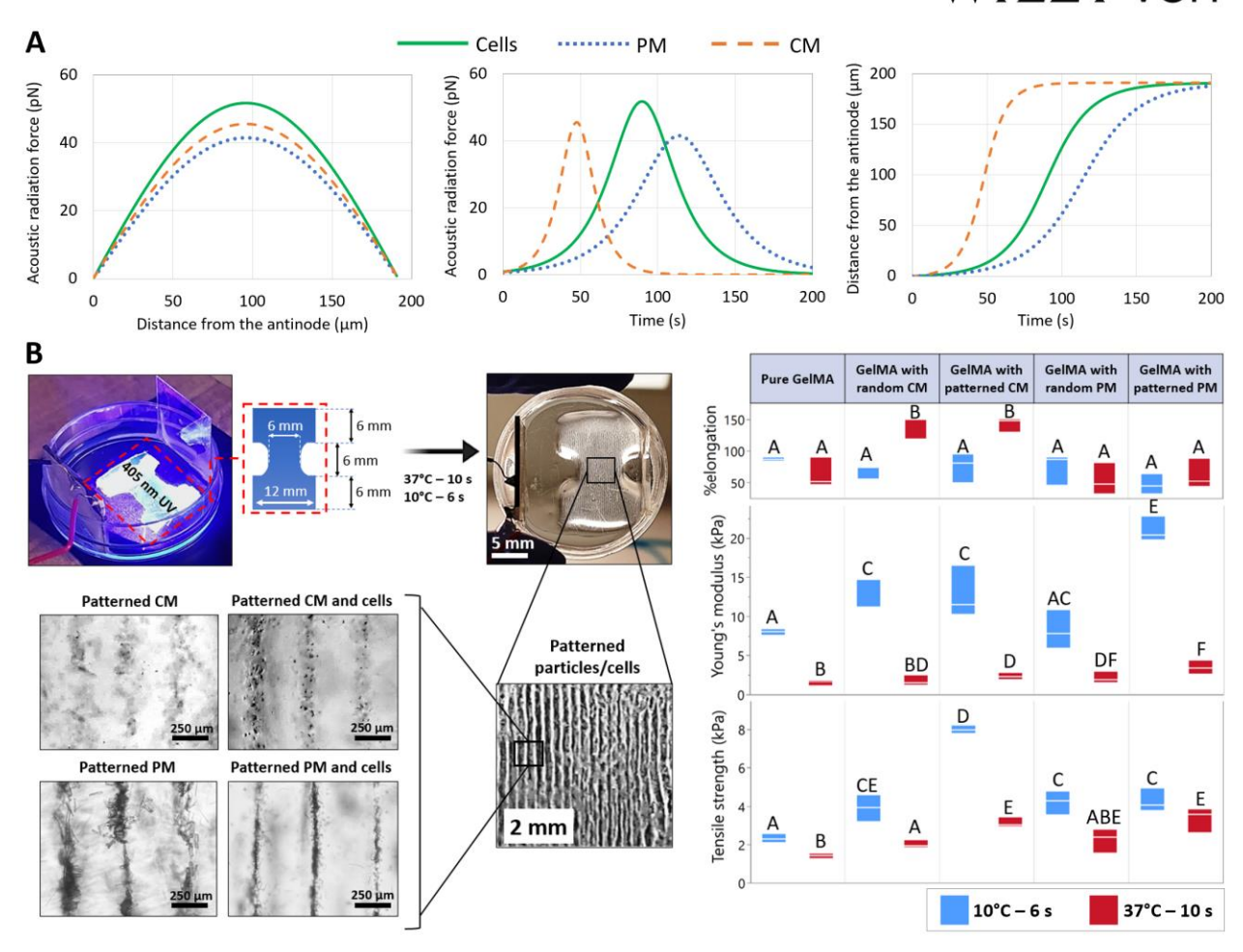


Figure 3. Patterning dynamics of cells and particles (CM/PM), and fabricated anisotropic constructs featuring planar patterning of cells and particles and their mechanical characteristics. A. Non-linear interdependencies of Fradiation, distance from the antinode and time. The Fradiation slowly increases as the cells/particles move from the antinode to the node and reaches the maximum amplitude mid-way between the antinode or the node. The radiation force is the highest for cells, followed by CM and PM. Due to an interplay between F_{radiation} and F_{drag}, the time to pattern is the fastest for CM, followed by cells and then the PM. B. UAB of dog bone hydrogels with patterned cells. A dog bone shaped mask was placed above a 405 nm UV lamp. A petri dish-based UPC consisting of cell-laden GelMA bioink in between a transducerreflector pair is placed atop the mask. After the appropriate duration of thermo-reversible and photocrosslinking, the dog bone constructs are photo-crosslinked to entrap the cells in the linear patterns. C. Results of tensile testing of pure and hybrid GelMA hydrogels. Addition of CM to the GelMA matrices enhanced stiffness in the 10°C-6 s formulation, and %elongation and tensile strength in the 37°C-10 s formulation. Patterning of CM further enhanced the tensile strength of both the formulations, indicating increased entanglement of collagen under physiological culture conditions. In contrast, addition of PM to GelMA, by itself, did not affect the %elongation or stiffness of the 10°C-6 s formulation, but PM patterning improved the stiffness. The addition of PM inherently improved the tensile strength of the 10°C-6 s

formulation, but only its patterning resulted in improved tensile strength in the $37^{\circ}\text{C-}10$ s formulation compared to pure GelMA. Letters A-F represent statistically significant difference (p < 0.05) from Tukey Post-hoc HSD. Error bars denote standard deviation.

The addition of CM to GelMA constructs of the 10°C-6 s formulation significantly increased the elastic modulus of the hydrogel but not its stretchability (i.e., percent elongation). In contrast, the presence of CM in the 37°C-10 s constructs improved their stretchability significantly but not their stiffness. Of note, the presence of CM improved the tensile strength of both hydrogel formulations, and the structural anisotropy induced by patterning the CM further increased the strength of these constructs. This effect was more pronounced in the 37°C-10 s formulation wherein the tensile strength of constructs with unpatterned CM and patterned CM was 2-times and 4-times higher, respectively, compared to corresponding pure GelMA constructs. The generally improved mechanical properties of 37°C-10 s constructs containing CM can be attributed to the secondary crosslinking of collagen in CM throughout the hydrogel matrix due to the physiological temperature (37°C) during UAB.

The addition of PM to the 10°C-6 s formulation, by itself, did not result in improvement in the stiffness, but PM patterning increased the stiffness by 2.5-times compared to the other groups. This increase can be attributed to the increased friction between the patterned PMs during stretching, similar to the behavior of fiber-polymer composites at higher fiber concentrations^[46]. In the 37°C-10 s formulation, however, the addition of PM and further patterning had a negligible effect on the hydrogel stiffness. In contrast to CM results, the addition of PM did not influence the stretchability of either formulation. The addition of PM to the GelMA matrix significantly enhanced the tensile strength of the 10°C-6 s formulation, but patterning did not result in further improvement. Patterning of PM in the 37°C-10 s formulation, however, did lead to higher tensile strength compared to pure GelMA. Some of these differences between CM and PM-based constructs, especially in the 37°C-10 s formulation, can be attributed to the lack of secondary crosslinking of PM within the GelMA matrix at physiological temperatures, unlike CM. Furthermore, the network of CM within the aligned arrays was denser compared to corresponding PM arrays due to faster alignment times of CM, which would have contributed to further improvements in properties due to CM patterning.

These results highlight how the mechanical functionality of the hydrogel (stretchability, stiffness, and strength) can be modulated, and in many cases, significantly improved by introducing

additives within the matrix. Ultrasonically induced patterning of those additives can further enhance these properties. It is also evident that the interplay between the additive chemistry and shape, matrix composition, and the biofabrication process parameters has a significant impact on the mechanical characteristics.

Next, we investigated the effects of these additives on the functional responses of encapsulated cells during the short and long-term maturation of the hybrid constructs. Post biofabrication, maturation of the constructs in culture is typically needed to impart the desired biofunctional characteristics.^[47] During long-term maturation, the cells proliferate, elongate, remodel the hydrogel matrix, and secrete new ECM. Herein, the hydrogel matrix needs to possess structural integrity to resist morphing due to cell anchoring and contraction, which will allow the biofabricated construct to maintain its shape fidelity. Hence, before commencing for long-term culture, we first evaluated characteristics of patterned GelMA hydrogels (37°C-10 s and 10°C-6 s formulations) containing hASC, with or without CM, over 1 week of culture. As can be seen in Figure 4A, hASC demonstrated good cellular alignment (i.e., elongation along the individual arrays) in the 37°C-10 s constructs, irrespective of the presence of CM. This could be attributed to the higher inherent matrix compliance, which allows the establishment of cell-cell contact necessary for cell alignment. However, these constructs lost their shape fidelity in culture relatively soon, exhibiting more than 50% isotropic contraction within a week, as indicated by the analysis of construct surface area in Figure 4B. This also resulted in significant reduction in inter-array spacing (Figure 4C). In contrast, the presence of patterned CM in the 10°C-6 s constructs resulted in significant improvement in cell elongation and proliferation along the arrays (Figure 4A), while the constructs maintained their shape fidelity over the week in culture (Figure 4B). The inter-array spacing also remained unchanged and similar to the theoretical estimate of $\lambda/2 = 375 \mu m$ (Figure 4C). In essence, the introduction of CM provided beneficial cell anchoring sites within a hydrogel matrix that by itself possessed limited matrix compliance. This is also evident in the array width, which is significantly higher than the other groups (Figure 4D). We further assessed the proliferation of hASC (measured via alamarBlue (aB) assay) in patterned 10°C-6 s constructs with and without CM (Figure 4E). While the % aB reduction was not significantly different between the two groups at Day 1, the constructs containing CM demonstrated significantly higher reduction (corresponding to cell proliferation) after a week. This only confirms the impact of the increased number of adhesion peptides in the matrix due to the CM. Taken together, these results clearly

demonstrate the enhanced functionality of patterned 10°C-6 s constructs with CM with respect to their mechanical properties, shape fidelity, and promoting cellular alignment and proliferation.

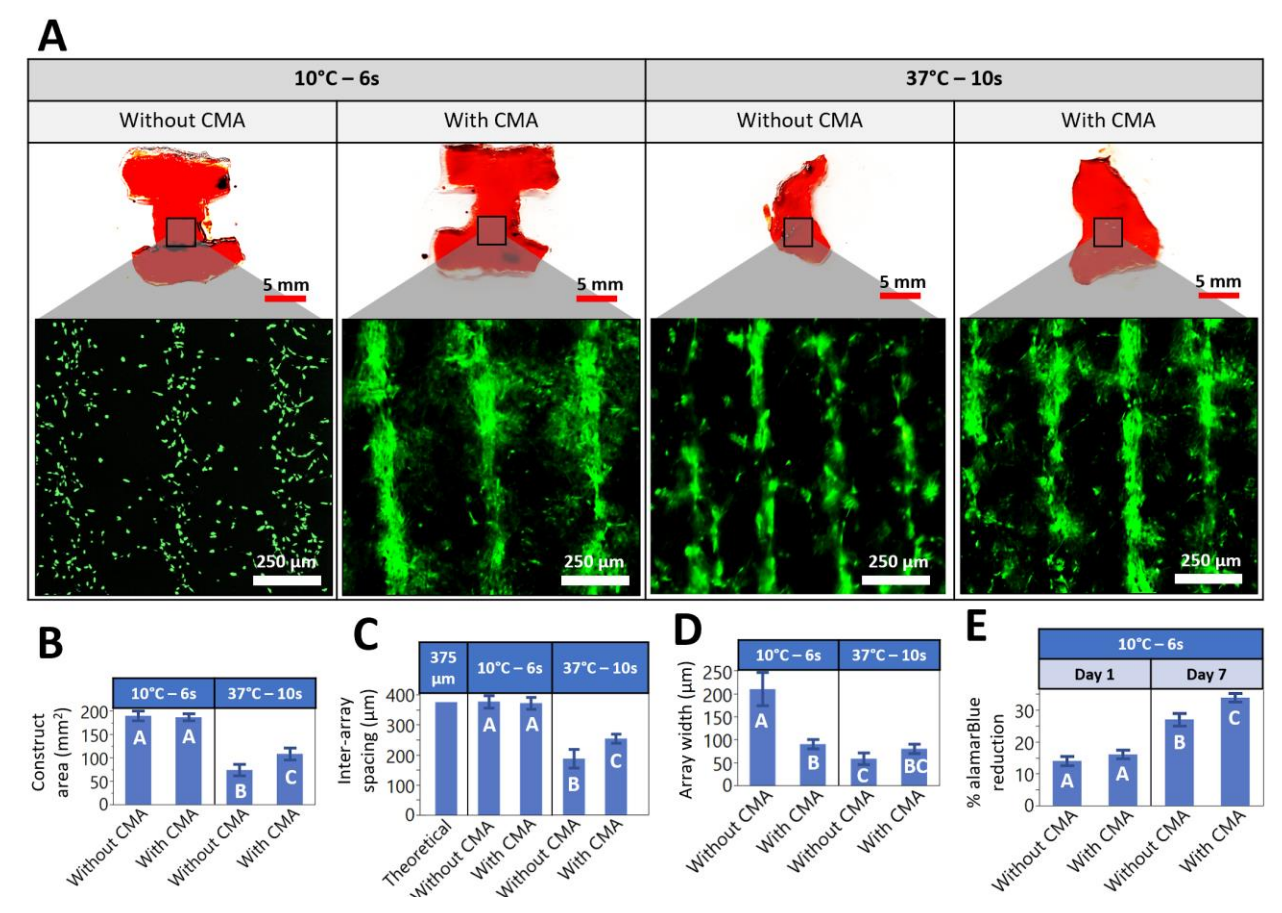


Figure 4. Investigation of morphology and metabolic activity of encapsulated cells and that of overall GelMA constructs featuring cell and CM patterning under longer term maturation. A. Morphology of hASC and GelMA constructs for the 10°C-6 s and the 37°C-10 s groups after a week in culture. The 37°C-10 s groups demonstrated cell proliferation along the arrays, but undergo significant matrix remodeling, leading to poor shape fidelity. In contrast, the 10°C-6 s formulations maintained shape fidelity, but only those featuring patterned CM demonstrated cell proliferation along the arrays (maintenance of anisotropy). B. Construct surface area measured in ImageJ, which demonstrates that only the 10°C-6 s maintained shape fidelity during short term culture, while the 37°C-10 s constructs underwent significant matrix contraction. C. Inter-array spacing measured in ImageJ, where the 10°C-6 s group maintained the spacing due to limited matrix contraction, while the spacing was lowered 37°C-10 s constructs due to matrix contraction. D. Width of the arrays within the constructs, wherein the array width is highest within the 10°C-6 s group without CM, since the cells proliferated in a haphazard way and lost their directionality over time. Other constructs demonstrated cell alignment and proliferation along the arrays, thereby exhibiting lower array width. E. Metabolic activity of the hASC-laden constructs as measured through %alamarBlue reduction. The

constructs containing CM demonstrated the higher metabolic activity compared to those without CM after a week in culture. In each plot, letters A-C represent statistically significant difference (p < 0.05) from Tukey Post-hoc HSD. Error bars denote standard deviation.

4. UAB of Constructs Featuring Anisotropic Cartilage Tissue

Following the optimization of the matrix composition and corresponding UAB parameters, we investigated the formation of anisotropic cartilage in patterned hybrid constructs subject to 4 weeks of static culture, which is relevant toward a variety of tissues such as the meniscus^[6] and the annulus fibrosus^[48]. Herein, we studied hybrid 10°C-6 s constructs (GelMA with CM or PM) containing hASC (cultured in chondrogenic differentiation media) or primary human chondrocytes. After 4 weeks, these constructs were evaluated for fidelity, cell morphology, and presence of collagen II (col II), the predominant ECM component in cartilage ^[49]. The corresponding results are shown in **Figure 5**. Owing to the optimized thermo-reversible and photocrosslinking, the constructs maintained their shape fidelity irrespective of the cell type or the additive.

Among the patterned constructs containing CM, the ones with hASC subject to chondrogenesis exhibited elongated and aligned morphology of both the cells and the cell-derived col II. This is evident in **Figure 5A** and confirmed by the corresponding analysis for length of cell processes and angular orientation in **Figure 5B**. The average length of processes for hASC (108.1 μ m), and the angular orientation remained within the -45° to +45° range for > 80% of the cells. In comparison, patterned constructs with CM and human chondrocytes exhibited a less elongated cell morphology (average length of processes = 36.2 μ m) and limited cell orientation (< 40% of cells within the -45° to +45° range). This difference between hASC that underwent chondrogenesis and primary human chondrocytes can be attributed to the limited cell-cell contacts due to smaller cell size of primary human chondrocytes (13.2±3.1 μ m) compared to hASC (21.1±3.3 μ m), as characterized via microscopic measurements (data not shown). The differing response of the two cell types to the adhesive cues provided by the CM may have also contributed to this difference.

In contrast, for patterned constructs containing PM, both cell types demonstrated similar aligned morphology and col II production. The cell alignment of chondrocytes in these constructs (average length of processes = $73.1 \, \mu m$) is markedly better than that in corresponding constructs with CM. A key contributing factor here is the higher aspect ratio of PM (approximately 4:1) compared to CM (approximately 1:1). The more prominently defined uniaxial attachment cues of the PM would have rendered increased alignment to the cells and cell-secreted collagen. In

comparison, the average length of processes for hASC-derived chondrocytes reduced to $80.4 \mu m$. These results indicate that the hybrid formulations containing CM were better-suited for eliciting cellular and ECM alignment from hASC-derived chondrocytes, while those containing PM were more appropriate for primary human chondrocytes.

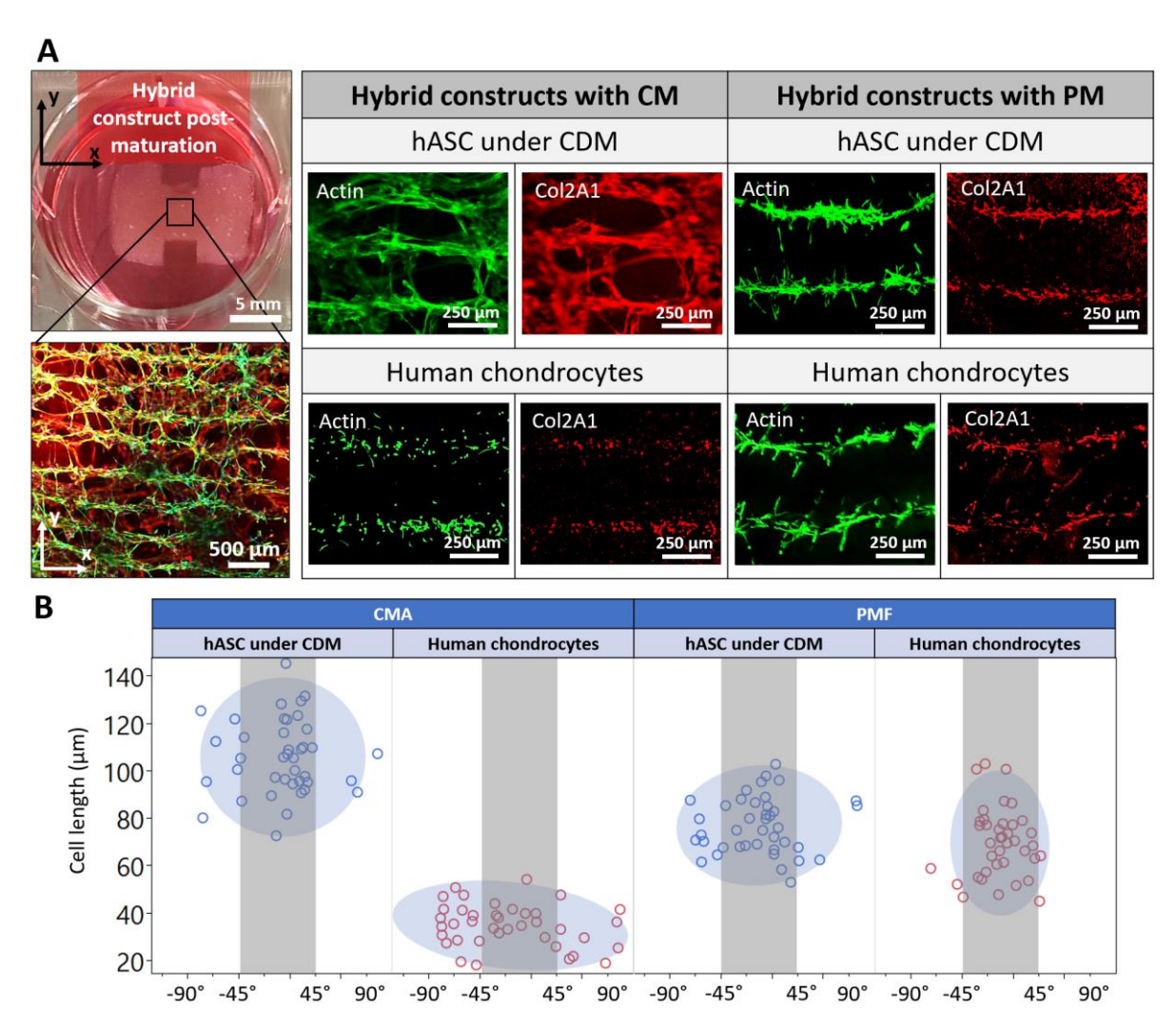


Figure 5. Synthesis of anisotropic cartilage via maturation (4 weeks in static culture) of constructs featuring UAB-driven planar patterning of cartilage forming cells and cell-adhesion promoting additives (CM and PM). A. Cell morphology (green, actin) and collagen production (red, Collagen II) of hASC under chondrogenic differentiation medium (CDM) and human chondrocytes after prolonged maturation within hybrid GelMA constructs containing CM or PM. For hASC with CM, both the cells and cell-derived Col II exhibited aligned morphology, which establishes the effectiveness of UAB method in producing anisotropic musculoskeletal tissues. For human chondrocytes along with CM, while the cells failed to establish an aligned morphology, the collagen was predominantly organized along a singular direction around the periphery of the cells. For constructs containing patterned PCL, both cell types demonstrated cellular and

Col II alignment. **B.** Length of cell processes and angular orientation (through image analysis in ImageJ) of hybrid constructs with hASC-derived chondrocytes or primary human chondrocytes. The CM were most suitable for hASC-derived chondrocytes, for the corresponding hybrid constructs feature highest length of the processes and the lowest variation in angular orientation (i.e., most cells are oriented along the arrays). In contrast, primary human chondrocytes exhibit long process length and more alignment along the arrays in hybrid constructs containing PM.

Overall, this study highlights the effectiveness of UAB in conjunction with appropriate material hybridization scheme in achieving anisotropy in engineered tissue constructs. The cellular elongation, angular orientation, and collagen deposition characteristics observed after maturation of these constructs (Figure 5) are comparable to the literature on the effects of topographical cues provided by aligned fibers/patterns created via electrospinning^[10], support-assisted bioprinting^[50], and soft lithography^[51]. In future, building upon the findings of this study and recent SAW-based literature about influences of acoustic stimulation beyond patterning^[52,53], we will investigate the effects of periodic BAW stimulation of UAB-patterned hybrid constructs during dynamic culture (i.e., in a perfusion bioreactor) on cell proliferation, directional migration, and ECM production, with the goal to further enhance the bulk anisotropy and biofunctionality of the constructs.

Next, we describe the versatility of UAB in being integrated with extrusion and stereolithography printing methods, and the scalability of UAB for the fabrication of thick, multilayered constructs featuring tailorable anisotropy.

5. Demonstration of Versatility and Scalability of UAB to Fabricate Complex and Physiological-scale Tissue Constructs

Most standalone process for tissue biofabrication are limited in their versatility and scalability, and appropriate hybridization is warranted to be able to produce truly biomimetic physiological-scale tissues^[54,55]. For the translation of UAB toward complex physiological scale tissue fabrication, we explored the hybridization of UAB with different configurations of established bioprinting process modalities utilizing the hybrid GelMA bioinks.

First, we demonstrate the integration of UAB with extrusion bioprinting to fabricate bilayered constructs featuring crisscross organization of hASC and CM (cells and CM aligned along 0° in layer 1 and along 90° in layer 2) and an intrinsic perfusable channel through the layers. The hybrid biofabrication schema is presented in **Figure 6**. A custom UPC consisting of an

orthogonal arrangement of transducer-reflector pairs was used, and different transducers were actuated for different layers of the extrusion-printed bioink. The radiation pressure distribution seen in the top and side views in each layer highlights the formation of nodes parallel to the transducer being actuated, thereby rendering cell and CM patterning along planes parallel to that transducer. Before printing the second layer, the first layer was allowed to thermo-reversibly crosslink at 10°C so that the cell and CM pattern in that layer was not affected by subsequent actuation of the other transducer for the second layer. After both layers were patterned and thermo-reversibly crosslinked at 10°C, a sacrificial serpentine vessel containing Pluronic was extrusion printed through the construct, followed by selective photocrosslinking of the GelMA in the construct using a projection mask with a square opening (20×20 mm²). The Pluronic slowly liquefied at 10°C and could be extracted to leave behind hollow vessel.

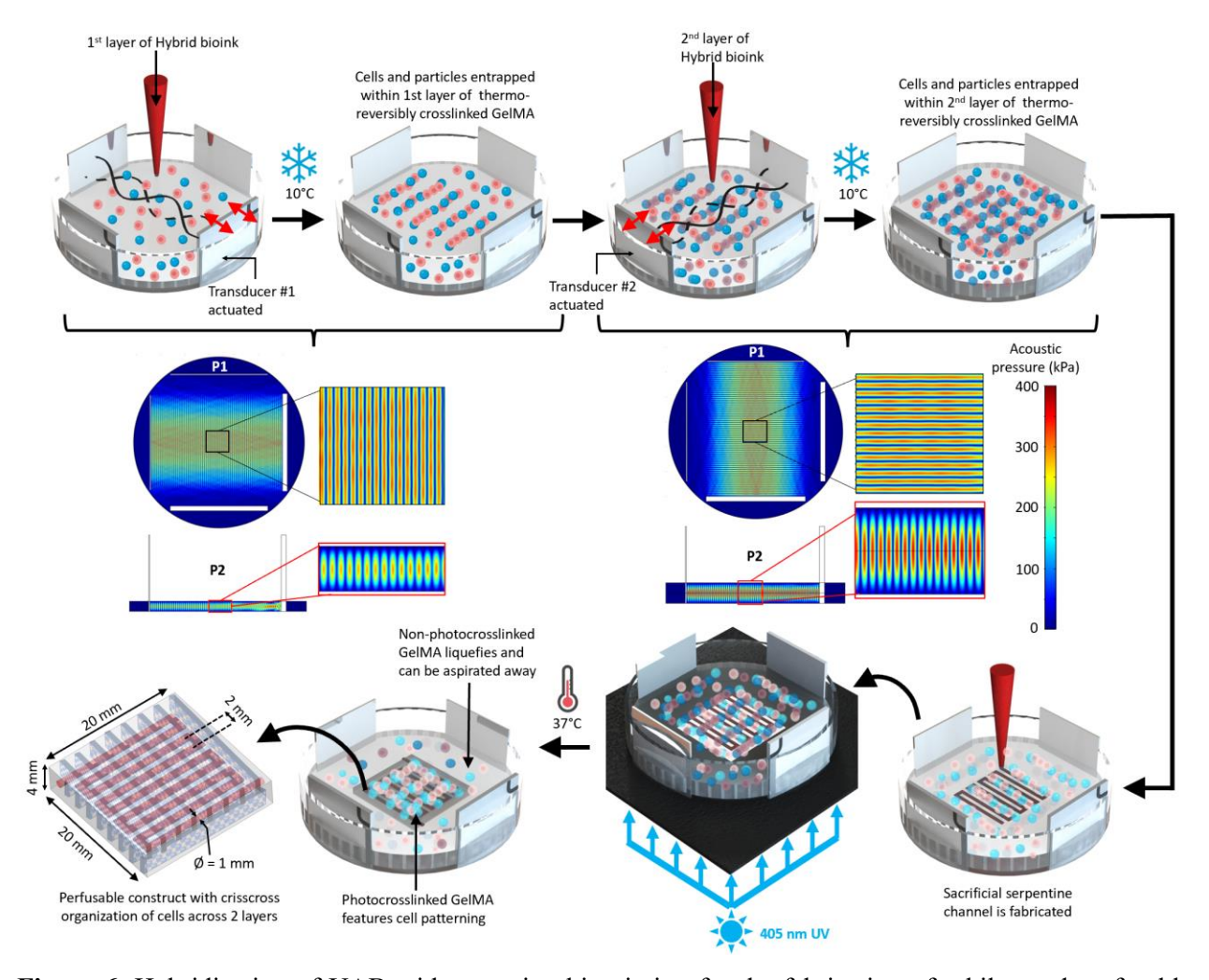


Figure 6. Hybridization of UAB with extrusion bioprinting for the fabrication of a bilayered perfusable construct with crisscross organization of cells and particles across the two layers. For the first layer, the

prepolymer GelMA containing cells and particles is added followed by actuation of transducer #1, causing the cells and particles to be patterned parallel to the transducer. This is also predicted by the straight lines of pressure nodes in the computational models. After thermo-reversible crosslinking (at 10°C) of the first layer, the prepolymer GelMA containing cells and particles is added to constitute the second layer. For this layer, transducer #2 is actuated, causing the cells and particles to be patterned in an orthogonal orientation. Note that the radiation forces generated by the actuation of transducer#2 are not sufficient to disturb the patterned cells in crosslinked layer#1 underneath, as the viscosity of that layer is much higher than that of the yet uncrosslinked layer #2. After layer#2 is thermo-reversibly crosslinked (at 10°C), the entire UPC is brought back to room temperature (24°C) and a serpentine channel of pluronic ink is printed using extrusion head. Next, the UPC temperature is dropped back to 4°C and photocrosslinked by UV exposure at 405 nm for 6 s, which allows liquification of the Pluronic vasculature, allowing it to be perfused out, while also photocrosslinking the GelMA to prevent any collapse of the vasculature.

The UPC was incubated at 37°C which caused the remainder of the thermo-reversibly crosslinked GelMA to get decrosslinked, leaving behind the final construct with the hASC and CM, patterned in an orthogonal orientation across the 2 layers (each 1.5 mm thick), and a perfusable channel for vasculature (**Figure 7**). This arrangement of cells and ECM components is characteristic of simple tissues as the skeletal muscle^[56], or even highly vascularized tissues such as the heart^[57]. Note that the primary purpose of these experiments was to demonstrate the versatility of the UAB approach, and the fabrication of functional constructs with endothelialized vessel networks in conjunction with anisotropic cell and ECM organization over long-term culture will be investigated in future studies.

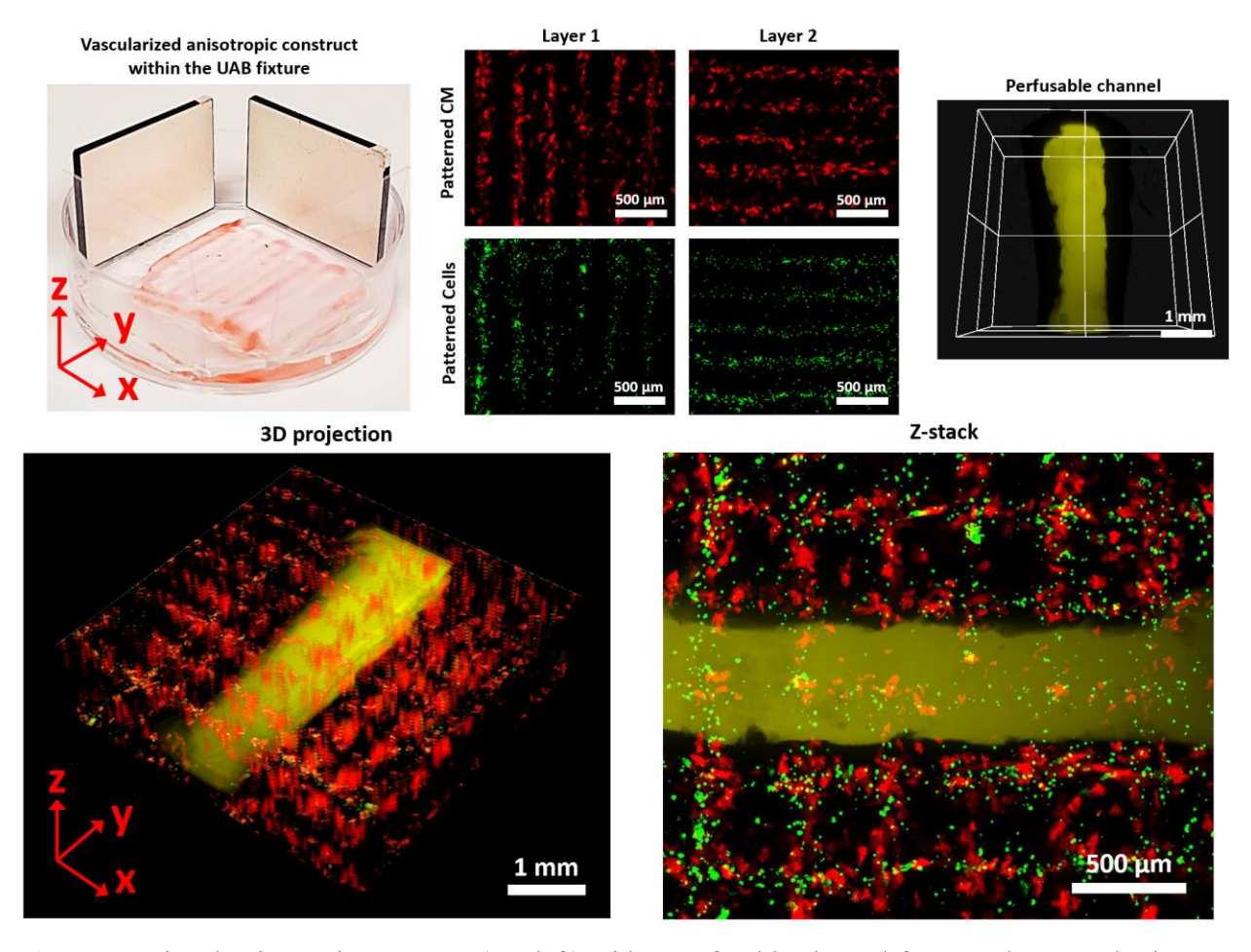


Figure 7. Printed anisotropic construct (top left) with a perfusable channel for vasculature and crisscross patterning of cells (green, labeled with Calcein AM) and CM (red, labeled with Dylight 650 NHS ester) as seen in the micrographs, confocal images and their projections. The vessel was perfused with gelatin containing NHS ester-fluorophore (Dylight 450) to allow its fluorescent imaging. The printed vessel runs through the crisscross patterned cells/particles as seen in the 3D projection view.

In the next study, to further demonstrate the versatility of UAB, we developed two different UPC configurations containing: 1) a semi-circular, rotary fixture with the transducer and reflector affixed at its ends, which can be rotated along the petri dish to modulate the cell-CM patterns imparted within the constructs, and 2) a circular instead of flat reflector to generate circular cell-CM patterns within the constructs. These UPCs were used in conjunction with top-down projection stereolithography. The two biofabrication schemes, and the fabricated constructs and their microarchitectural characteristics are shown in **Figure 8**.

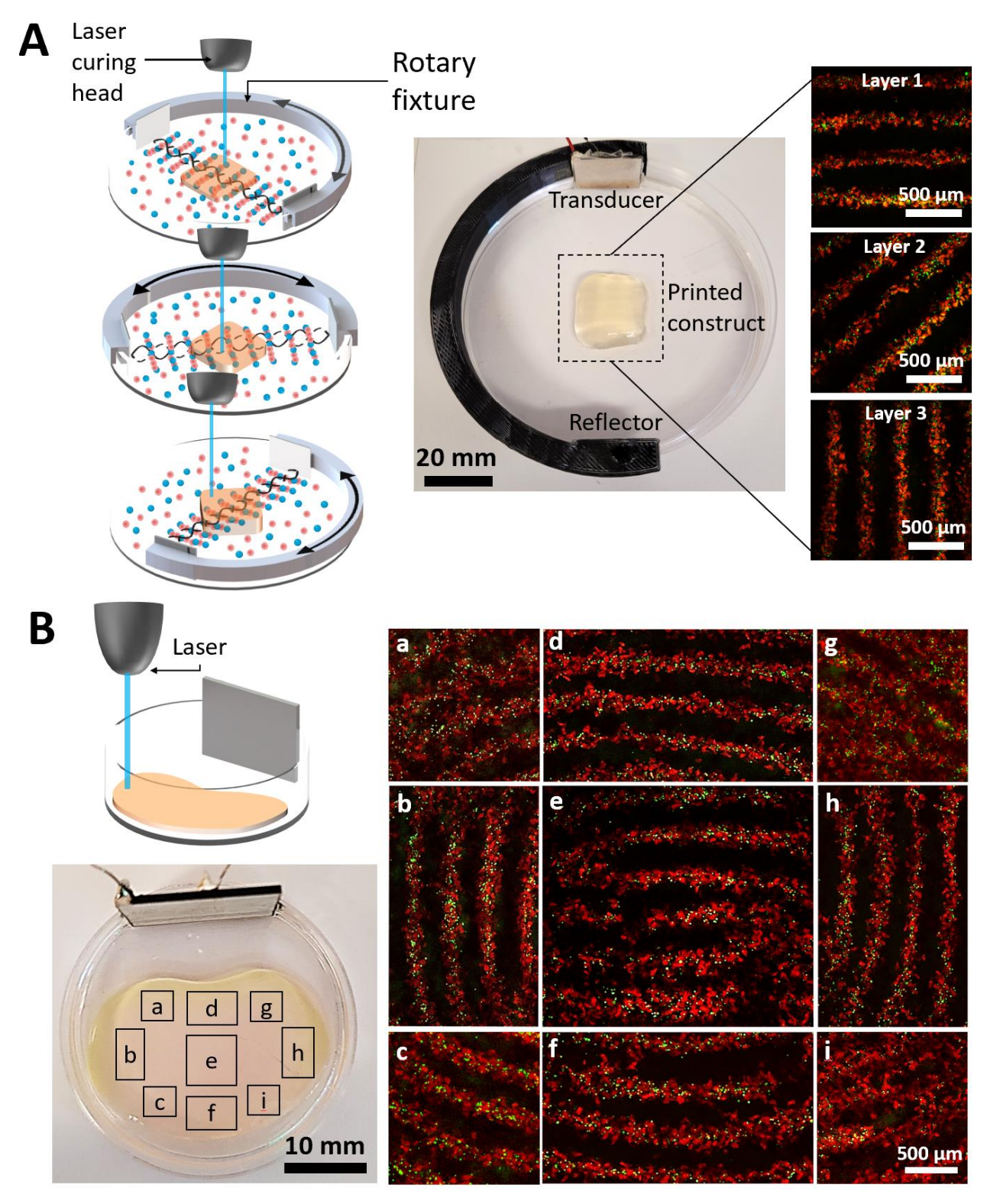


Figure 8. Hybridization of UAB with laser-assisted stereolithography printing. **A.** UPC with the rotary fixture for the fabrication of constructs with custom patterning across different layers using a single pair of transducer-reflector. For example, hASC (stained green, Calcein AM) and CM (stained red, Dylight 650 NHS ester)-laden GelMA bioink is added to the petri dish and the fixture is rotated along 0°, 45° and 90°

for layers 1-3, respectively to fabricate the three-layered construct shown on the right. We added a UV absorptive dye^[58] to allow photocrosslinking after the patterning in each layer to minimize over-crosslinking of the layers underneath. **B.** Fabrication of annulus fibrosus-shaped construct with circular hASC and CM patterning achieved using a circular reflector. The cell and CM patterning (as shown in the selected regions a-i) mimics the circumferential cell and ECM organization found in the native tissue^[6,48].

Using the UPC with the rotary fixture setup, a three-layered construct (each layer being 1.5 mm thick) featuring 0°-45°-90° patterning of hASC and CM was fabricated (**Figure 8A**). While we chose three angular orientations, owing to the free rotation of the rotary fixture, virtually any angular orientation can be imparted within the constructs. This will be highly relevant to the fabrication of tissues such as the cardiac tissue where the fiber orientation can vary from 0° to +80° in the myocardium to the endocardium, respectively^[1,2]. In the second UPC configuration, the circular reflector served as a simple yet effective tool to impart circular patterning of functional constituents within a single-layered (1.5 mm thick) construct to mimic the native microorganization in an annulus fibrosus-shaped 3D construct (**Figure 8B**). This is similar to the physiological distribution of cartilage cells and ECM in the native tissue^[6,48].

It should be noted that in the study with the rotary fixture, the dual crosslinking property of GelMA could not be exploited as the orientation of the transducer needed to be changed after every layer, and rotating the transducers while the GelMA was only thermo-reversibly crosslinked would have damaged the hydrogel. Rather, the cells and CM were patterned in each GelMA layer at 37°C and photocrosslinked right after. After photocrosslinking of a layer, the orientation of the rotary fixture was changed, and fresh bioink for the next layer was printed and patterned. To prevent excessive photocrosslinking of the layers underneath while the top layer was being photocrosslinked, a UV absorptive dye^[58] was added to the bioink (see details in the methods section). As such, once the cells/bioadditives are ultrasonically patterned in a layer of bioink and that layer is crosslinked, due to its increased viscosity, the pattern is entrapped and not adversely affected by the printing, acoustic stimulation, and crosslinking of a new layer of yet uncrosslinked bioink on top. Conversely, given the lateral mode of propagation of the bulk acoustic pressure waves, the presence of a crosslinked layer underneath does not influence the ultrasound parameters (e.g., frequency, voltage amplitude, actuation duration) and the radiation pressure amplitudes (computational results in Figure 6) required to achieve patterning of cells in a new uncrosslinked bioink layer^[36]. Thus, the use of a rotary fixture represents a facile method for the real-time

manipulation of the orientation of the cells. In future studies, we will optimize the design of the rotary fixture such that it could be rotated without damaging the thermo-reversibly crosslinked GelMA.

Appropriate automation and hybridization of UAB process are key to future translation prospects of this technology. The aspect of automation can relate to the sequential or harmonic actuation of different transducers (such as in the orthogonal transducer arrangement used for perfusable anisotropic tissue printing) for different layers via the use of high frequency relays^[35] or an on-demand real-time change of the spatial orientation of the transducers using a motorized rotary fixture. Furthermore, the amplitude or duration of transducer actuation can be altered depending on the desired width of the arrays^[36], and the frequency can be varied to generate different inter-array spacing^[35,36] in different layers, driven by the desired tissue application. The actuation of transducers and any associated process changes (frequency, amplitude and duration of actuation) can be implemented through the inbuilt microcontroller system of the printer or an external microcontroller capable of establishing communication with the printer. As for hybridization, the appropriate combinatorial processes and their hybridization schemes need to be selected depending on the material requirements, complexity of the architecture, and other process attributes such as the throughput, biocompatibility etc. [54]. In future studies, we will investigate the hybridization of the rotary UPC with bottom-up digital light projection printing, which has previously demonstrated ultra-high precision ($50-100 \mu m$) bioprinting of perfusable vascularized constructs^[58]. Ultimately, exploring the synergistic application of such strategies can enable to expand the range of achievable microarchitectural complexities, including patterns with spatially varying gradients, relevant for biomimicry with higher processing efficiency and reproducibility.

The interactions between the material-process-structure will be another important factor to consider in future studies. We plan to explore alternate hydrogel matrices^[59,60] such as collagen, hyaluronic acid, chitosan or fibrin and their appropriate combination to facilitate anisotropic cell proliferation and ECM production, keeping in mind that changes in the materials would affect the radiation forces acting on the cells and additives and the time required to pattern them. Sterilization processes could also affect the material properties such as the molecular weight and viscosity^[61], which can in-turn affect the patterning characteristics and subsequent proliferation of the cells and the production of ECM. Future studies will also explore different types of micro and nanofiber additives to hybridize the bioinks to facilitate anisotropic tissue fabrication^[62]. Herein, one important factor to consider is that acoustic fields are more appropriate for manipulation of particles

in the micrometer scales (usually $> 1~\mu m$) due the size constraints associated with the viscous penetration depth^[26]. However, nanofibers could still be patterned if one of the dimensions exceeds the penetration depth. Alternatively, nanoparticles could be ionically or covalently tagged onto microparticles and patterned using UAB, followed by selectively dissolving away the microparticles to indirectly pattern nanoparticles within the matrices. To account for any changes in UAB process necessary for different materials, the road map established by the present study will be used, wherein we will first optimize the matrix formulation to enable cell attachment while maintaining construct fidelity, prior to moving forward towards long-term construct maturation.

6. Conclusion

This work represents advancements along both biomaterials and biofabrication fronts, where new ultrasound-assisted fabrication and bioprinting processes are used in synergy with new hybrid hydrogel formulations to create complex, anisotropic, physiological-scale constructs. In the first study, we optimized the biochemical and mechanical characteristics of GelMA hydrogel constructs with ultrasonically-patterned cells to facilitate cell and ECM alignment. Herein, the effects of thermo-reversible crosslinking (by controlling the pre-photo-crosslinking solution temperature) and photo-crosslinking (by controlling duration of UV exposure) on the microstructure, mechanical and biological properties of resulting GelMA hydrogels were characterized. Enhancing the extent of thermo-reversible crosslinking increased the number of structural reinforcements within the hydrogel matrix, thereby improving the stiffness and long-term robustness of the hydrogels. However, it was evident that the extent of thermo-reversible crosslinking needs to be carefully optimized to achieve the desired bio/mechanical properties in the hydrogels, as demonstrated by the results of maturation of pure GelMA hydrogels featuring patterned hASC. The biochemical and mechanical properties of GelMA hydrogels were further enhanced upon the addition of CM or PM (hybrid hydrogel constructs), which provided additional adhesive cues for cell alignment and strengthened the matrix to help maintain shape during long-term culture. The results of long-term maturation of constructs clearly demonstrated that hybrid constructs, especially the constructs formulated under cold conditions, were superior to pure GelMA counterparts in maintaining construct fidelity and promoting cell alignment and cell-secreted anisotropic collagen network within the constructs. From these results, it was evident that human chondrocytes exhibit a less elongated morphology and demonstrate attachment over a smaller range of matrix stiffness compared to hASC. Using novel UPC configurations and their appropriate process hybridization

with extrusion printing and stereolithography, we also demonstrated fabrication of complex constructs featuring anisotropic cell and additive organization across multiple layers along with intrinsic perfusable channels for vasculature development. The new hybridization schemes for bioink and processes and their appropriate synergy demonstrated in this work will further research advancements in biomimetic tissue engineering research.

7. Methods

UAB Setup: All UPCs in this work consisted of piezoelectric transducers with 2 MHz resonant frequency (SMPL20W15T1R111, Steiner and Martins Inc., Davenport, FL). The UPC to create the dog bone constructs comprised of a single transducer attached onto a non-treated petri dish (\emptyset = 35 mm, CLS430588, MilliporeSigma), and a glass slide (length = 18 mm, thickness = 0.2 mm) attached at the opposite end. To ensure the formation of a SBAW, the distance between the transducer and reflector (L) was set to 21 mm; this is an integer multiple of λ /2 (λ = 750 μm at 2 MHz in water; speed of sound (c) = 1500 m/s)), which is the distance between successive pressure nodes. To actuate the transducer, a sinusoidal voltage was generated via a function generator (Keysight Technologies Inc., CA) and amplified via a high frequency amplifier (240L, Electronics & Innovation Ltd., NY).

For perfusable bilayered anisotropic construct fabrication, the UPC consisted of two transducer-reflector pairs (L = 21 mm; integer multiple of λ /2) positioned orthogonally (Figure 7). For the rotary UPC, a custom ABS fixture was designed and 3D printed to conform to the outer periphery of a petri dish (Ø =100 mm) to be able to easily rotate at different angles to fabricate the anisotropic constructs. The transducer and reflector were attached to the end of the fixture separated by L = 87 mm (integer multiple of λ /2). For creation of circular patterning in the annulus fibrosus-shaped constructs, the UPC for the creation of dog-bone shaped constructs was used, but with circular face of the petri dish as the reflector instead of a glass slide.

Formulation of Pure GelMA Photoink: The GelMA used in this study was purchased in a lyophilized form (80% degree of substitution (DOS), 900496, Millipore Sigma). The consistency of DOS across different purchased batches was verified using 1 HNMR spectroscopy $^{[43]}$ to be within $\pm 7.5\%$. The lyophilized GelMA was constituted at 5% w/v in phosphate buffered saline (PBS) and the photoinitiator Lithium phenyl-2,4,6-trimethylbenzoylphosphinate (LAP) added at a concentration of 0.25% w/v to formulate the pure GelMA photoink.

Formulation of Hybrid GelMA Photoinks Containing CM or PM: Hybrid GelMA photoinks were formulated by constituting CM or PM at 1 mg/ml within pure GelMA photoinks. To fabricate CM, collagen I (4mg/ml, RatCol®, 5153, Advanced BioMatrix, Carlsbad, CA) was dissolved in cold media (4°C) in a 15 ml centrifuge tube, followed by rocking at 30 Hz, 60 Hz or 90 Hz for 1 h to achieve different size CM (Figure 2D). The solution containing CM was then centrifuged at 3000 rpm for 5 min to formulate a pellet of the microaggregates. The supernatant was aspirated, and CM reconstituted within the relevant volume of pure GelMA photoink to formulate the hybrid photoink.

To fabricate PM, PCL scaffolds (5 mm × 5 mm) featuring uniaxially aligned microfibers were fabricated first via melt blowing. The melt blowing setup and processing is described elsewhere [11]. The key melt blowing process parameters included die to collector distance (DCD = 150 mm), fiber deposition offset (FDO = 80 mm), and surface velocity of the collector (SVC = 150 m/min or 700 m/min) to achieve different fiber diameters (Figure 2E). Post fabrication, the scaffolds were treated with NaOH to improve hydrophilicity. The microsectioning of the constructs was then performed similar to the study by Omidinia-Anarkoli et al.^[63] The constructs were embedded in optimal cutting temperature compound (OCT, AGR1180, Agar Scientific, Essex, UK) within Cryomold® molds (15 x 15 x 5mm, AGG4582, Agar Scientific), followed by cryofreezing on dry ice (- 80°C) for 4 h. The fiber orientation was ensured to be perpendicular to the cutting direction. The samples were then cryosectioned (50 or 100 µm) such that monodisperse fibers could be obtained. The PM, while still embedded and frozen in OCT compound, were transferred to 50 ml tubes and stored in a -80°C freezer until further use. On the day of experiments, PBS was added to the samples dissolve the OCT compound and disperse the PM, followed by vortexing for 20 s and repeated pipetting to break apart any entangled PM. The solution was then centrifuged at 4000 rpm for 5 min followed by aspiration of the supernatant and resuspension of the PM in fresh PBS. The process of centrifugation, aspiration, and resuspension was repeated thrice to remove all traces of OCT. Finally, the PM pellet was reconstituted into the appropriate volume of GelMA solution to formulate the hybrid photoink.

Cell Culture and Bioink Formulation: The hASC (StemPro™ R7788115, Thermo Fisher) were cultured (37°C, 5% CO₂) in MesenPRO RSTM basal medium and growth supplement (12746012, ThermoFisher) and 1% L-Glutamine (ThermoFisher). Chondrocytes (CELLvoTM, StemBioSys, San Antonio, TX) were cultured in DMEM containing 15% FBS and 1% L-Glutamine. Media changes for all cells were performed every 48 h until 80% confluency was reached. To maintain consistency across all studies in this work, all cells were used at Passage 2 for construct fabrication.

For studies involving cellular constructs, the cells were passaged using 0.25% Trypsin-EDTA (Millipore Sigma) and centrifugated at 300 g for 5 min to create a cell pellet, which was then reconstituted in pure or hybrid GelMA photoinks to create the cellular bioink. The cell concentration was kept constant at 10^6 cells/ml throughout all the studies.

Computational Modeling of Acoustic Pressure Distribution in UPC: The 3D finite element analysis (FEA) model was setup in COMSOL Multiphysics® (Comsol Inc., MA) in its acousticpiezoelectric interaction module^[37]. The boundary conditions and material attributes were established as per Figure 1B. To the domain containing bioink, the attenuation of ultrasound (α in dB/m) was assigned to be dependent on frequency ($\alpha = 12f$, where f is frequency)^[64]. To the boundaries of bioink domain in contact with the petri dish or the air, the acoustic impedance (Z_m $= \rho_m c_m$, where ρ_m is mass density of the contact medium and c_m is speed of sounds in the medium) was defined. The contact medium comprised of petri dish plastic ($\rho_m = 1070 \text{ kg/m}^3$ and $c_m = 2230$ m/s) at the sides and bottom, and air at the top (ρ_m = 1.22 kg/m³ and c_m = 343 m/s). To the transducer, in the solid mechanics and electrostatics submodule, transducer attributes we applied as specified by the manufacturer^[36]. Herein, the isotropic structural loss factor was 1/1800, and the dielectric dissipation factor was 0.4. Further, the transducers equations were defined in the stress charge form: $T = c_E S + e^T E$, where T is transducer stress, S experienced strain and E is the applied electric field, and c_E and e^T were the stiffness and coupling matrices. Herein, the coefficients for stiffness and coupling matrices were $c_{E(11)} = c_{E(22)} = 86$ GPa, $c_{E(33)} = 73$ GPa, $c_{E(66)} = 172$ GPa, and $e^{T}_{(31)} = e^{T}_{(32)} = -12.4 \text{ C/m}^2$, $e^{T}_{(33)} = 23.36 \text{ C/m}^2$. To the transducer, a harmonic perturbation at 2 MHz and 50 Vpp was applied at the side contacting the bioink, and the opposite surface was defined as ground with a fixed constraint. Herein, a triangular mesh was used with element size less than 0.03 mm (i.e. $< \lambda/10$ at 2 MHz^[65]).

Fabrication of Constructs to Investigate the Effects of Different Thermo-reversible and Photocrosslinking Conditions on the Hydrogel Microstructure and Cell Attachment: These constructs were fabricated for studies discussed in Figure 2A and B. The constructs were cylindrical in shape, fabricated within non-treated 24-well plates. The fabrication procedure was kept consistent with that used with ultrasound-assisted patterning within UPC chamber. To fabricate constructs at 37°C, acellular (for microstructural analysis using CryoSEM) or cellular (containing hASC; for cell attachment and elongation analysis) pure GelMA photoink at 37°C was added within the wells at 500 µl/well. To fabricate constructs at 37°C, the 24-well plate was transferred over a UV lamp (10 mW/cm²) and photocrosslinked at 6 or 10 s of UV exposure. To fabricate constructs at 10°C, the well plate was placed over a temperature-controlled plate (Z176664, Millipore Sigma) and thermo-reversibly crosslinked for 5 min prior to transferring over the UV lamp and photocrosslinking for 6 and 10 s. The crosslinked acellular constructs were extracted using a pair of forceps for CryoSEM analysis, while the cellular constructs were left within the wells and 1 ml of cell culture media added atop. Media changes over the cellular constructs were performed every day until day 3 (considering the constructs were fabricated at day 1).

CryoSEM of GelMA Samples and Determination of Porosity: The cryogenic scanning electron microscope (7600F, ALTO, Gatan, JEOL Ltd) was prepared for imaging by cooling-down the anticontaminators and the chambers for the sample preparation and SEM stage to -140°C and -165°C, respectively. The GelMA samples were loaded onto the holding jigs and rapidly frozen in slush nitrogen. The samples were then freeze-fractured inside the sample preparation chamber, then heated until -90°C and sublimed for 5 min, followed by sputter coating under argon at 10 mA for 4 min. The sample holder jig with the sample was transferred to the imaging chamber. During imaging (at 1 kV), the cryoSEM was maintained at 4×10-6 mbar. The pore sizes were determined from CryoSEM images (3500X magnification) using a custom algorithm in MATLAB that we developed in our previous work^[43].

Assessment of Viability and Elongation of Cells in Pure GelMA Constructs under Different Thermo-reversible and Photocrosslinking Conditions: For the study shown in Figure 2, the media above the constructs in the 24-well plates was extracted and 1 ml of PBS containing Live/Dead® assay reagents (L3224, Thermo Fisher) at a concentration of 0.25 μl/ml for calcein-AM and 1 μl/ml of ethidium homodimer-1 added. The constructs were then washed and imaged using fluorescence microscopy (SP8, Leica Microsystems). Analysis of cell length was performed in ImageJ^[66].

Fabrication of constructs with or without ultrasound-assisted patterning of additives for mechanical testing: For mechanical testing (acellular constructs containing CM/PM), the dog-bone shaped hydrogel constructs with or without cell/particle patterning were fabricated using mask projection lithography. The constructs featured only photocrosslinking (37°C groups), or a combination of thermo-reversible and photo-crosslinking (10°C groups).

For the constructs fabricated at 37°C, the UPC was placed over a UV lamp (10 mW/cm²) with an interfacial dog bone-shaped mask (Figure 3B). Then, 2 ml bioink containing appropriate cells and/or CM or PM was dispensed into the UPC. A burst voltage signal (50 Vpp, 2 MHz, 1 s actuation followed by 1 s pause) was then applied to the transducer via the function generator and amplifier. This ultrasound actuation regimen has been previously demonstrated to be non-deleterious to cells^[35,36]. The bioink was selectively exposed to UV (6 s or 10 s) after 5 min of ultrasound actuation; the transducer remained actuated for 10 min to be consistent with the hydrogels fabricated at 10°C.

To fabricate constructs at 10°C, the UPC was placed over the temperature-controlled plate. First, 2 ml of bioink formulated at 37°C was introduced into the UPC and the transducer actuated. After 5 min of ultrasound actuation, the UPC was cooled down to 10°C for an additional 5 min to induce thermo-reversible crosslinking while the transducer remained actuated. As a result, the cells and particles were entrapped in their patterns, and the UPC was transferred over to the UV lamp, followed by selective photo-crosslinking of the bioink. The UPC for both the 37°C and 10°C groups were placed within a larger petri dish (Ø 100 mm, 25 mm deep) and incubated (37°C, 5% CO₂) for 30 min to liquefy any non-photocrosslinked GelMA, which was then aspirated.

For the constructs without ultrasound patterning, the transducers were not actuated during the construct fabrication process, while other temperature control steps were kept the same as those for 10°C and 37°C groups with ultrasound patterning. The distance between the lamp to the base of the UPC was kept consistent at 10 mm across all studies.

Tensile testing of dog-bone shaped hydrogels with or without patterning of additives: For the acellular dog bone-shaped hydrogel constructs to be evaluated in tensile testing, post fabrication, the constructs were incubated at 37°C in media for 30 min to allow for stress relaxation before testing. This also allowed recapitulation of culture conditions for the cells in longer term maturation studies. During testing, the constructs were affixed lengthwise onto a 5 N load cell on a universal testing system (5944, Instron, Norwood, MA), and a constant tensile strain rate of 0.125 mm/mm/min was applied. From the derived stress-strain curve, the elastic modulus was calculated as the slope of the region between 0-10% strain, the tensile strength corresponded to the peak of the curve, and % elongation was measured corresponding to the strain at the breakage point.

Assessment of shape fidelity and cellular activity in hybrid GelMA construct during short term culture: This study corresponded to the results described in Figure 4, and was performed on dog bone-shaped hydrogels laden with hASC and CM. The bioink for the study was prepared by passaging the hASC (passage 2) and centrifugating to create a cell pellet. The cells were then reconstituted at a concentration of 10⁶ cells/ml in hybrid GelMA photoink containing CM at 1mg/ml. The fabrication procedure was the same as that used to create the constructs for mechanical testing. Post fabrication, the dog bone hydrogel (pure and hybrid) constructs were transferred to 6well plates and 4 ml of relevant media added atop. Each day, old media was replaced with 2 ml of fresh media to prevent any accidental damage to the constructs during the aspiration. The constructs were cultured up to a week, and were then evaluated for the change in surface area in ImageJ^[66]. The constructs were also immersed in 3 ml of PBS containing Live/Dead® assay reagents (concentrations mentioned in previous sections) and imaged using fluorescence microscopy and evaluated in ImageJ for cell morphology changes. Separate constructs were also evaluated for their metabolic activity using alamarBlue® (aB) assay reagent (ThermoFisher). At day 1 (day of construct fabrication) the supernatant media from the construct wells was replaced with 4 ml of media supplemented with aB reagent at 10% v/v. After 4 h of culture under gentle rocking, three 1 ml samples were extracted from each well and analyzed for absorbance (Tecan, Männedorf, Switzerland) at 570 nm and 600 nm excitation and emission wavelengths, respectively. The % aB reduction was determined by normalizing the absorbance data to the acellular control. The constructs were washed, and 4 ml of fresh media was added again. The constructs were then reevaluated for % aB reduction at day 7 using the same protocol.

Synthesis and evaluation of anisotropic cartilage tissues: These methods corresponded to results presented in Figure 5. Herein, the 10°C-6 s group was used, since this group had featured cell attachment and proliferation in addition to maintenance of shape fidelity over 4 weeks. The dog bone-shaped constructs were fabricated using hybrid (CM or PM at 1 mg/ml) and cellular (hASC or primary human chondrocytes at 10⁶ cells/ml) GelMA. Since the constructs were to be evaluated for anisotropic cartilage formation, they were cultured for 4 weeks in 6-well plates with 4 ml of CDM (for constructs containing hASC, 411D, Millipore Sigma) or chondrocyte media (for constructs containing primary human chondrocyte). Media changes were performed every 48 h. After 4 weeks, the constructs were fixed in 4 ml of 2% paraformaldehyde containing 0.2% TritonX for 15 min. The constructs were then blocked overnight in PBS containing 3% (w/v) bovine serum albumin (Millipore Sigma). Next day, anti-Col II primary antibody (ab34712, Abcam, Cambridge, UK) was added at a concentration of 5 µg/ml, followed by incubation under stirring at 22°C for 24 h. The constructs were then washed thrice with fresh PBS, followed by addition of 4 ml of PBS containing 0.1% TritonX. Next, 125 µl Phalloidin (A12381, ThermoFisher Scientific), 125 µl NucBlue (R37605, Thermo Fisher Scientific) and secondary antibody at a concentration of 1 µg/ml (A-11012, Invitrogen, Carlsbad, CA) was added, followed by incubation at ambient condition (22°C) for 4 h. The constructs were then again washed thrice with fresh PBS, and imaged using a confocal microscope (Fluoview 3000, Olympus, Tokyo, Japan).

Hybridization of UAB with extrusion and stereolithography bioprinting for demonstration of scalability and versatility: The versatility and scalability experiments were performed on hybrid bioink containing fluorescently labeled hASC and CM. The cells were stained with neutral red dye (552-24-2, Millipore Sigma) added at a concentration of 10 μg/ml to the cell culture media, while the CM were dyed using an NHS ester fluorophore dye (Dylight 650, Thermo Fisher) added at a concentration of 10 μl/ml to the neutralization media. The cells and CM were stained for 30 min, and excess dyes were removed by centrifugation of the passaged cells (at 500 g) or CM (3000 rpm) in suspension, followed by resuspension in PBS. This procedure was repeated twice prior to constituting the bioink following the protocols described earlier.

To fabricate the constructs featuring crisscross cell patterning and perfusable channels, 1.5 ml of hybrid GelMA bioink was added to the UPC containing the orthogonal transducer orientation, followed by ultrasound actuation (2 MHz, 50 Vpp, burst mode) of one of the transducers and

thermo-reversible crosslinking at 10°C for 5 min to entrap the cells and CM in their organized patterns in the layer. The second layer was then fabricated by adding 1.5 ml of fresh bioink and actuating the orthogonal transducer to impart a crisscross patterning of hASC and CM in the two layers. After patterning of the cells and thermo-reversible crosslinking of the second layer, the entire chamber was brought back to room temperature (24°C) and temperature verified using temperature sensor (TG267, FLIR). The serpentine channel (geometry highlighted in Figure 6) was then extrusion printed (BioX, Cellink) using a sacrificial ink at the interface of the two layers at 80 psi and 3 mm/s. The sacrificial ink comprised of 20% Pluronic (F-127, 9003-11-6, Millipore Sigma) in DI water. After printing the sacrificial channel, the chamber was brought back to 4°C for 5 min followed by UV crosslinking at 405 nm for 6 s to allow the Pluronic to liquefy. Thereafter, the Pluronic was flushed out gently using a syringe filled with PBS, while preventing the collapse of the hollow channels left behind by photocrosslinking the GelMA. The chamber was then brought back to 37°C to thermally decrosslink the non-photocrosslinked GelMA, leaving behind the final perfusable anisotropic construct. Prior to imaging, the hollow channel was perfused at room temperature with a 1% w/v gelatin solution containing an NHS-ester fluorophore at 10 μl/ml (Dylight 450 NHS Ester, Thermo Fisher). Due to the formation of amide linkages between the ester in the fluorophore and primary amines in gelatin, and due to the thermo-reversible crosslinking of gelatin within the channels, the fluorophore could remain constrained within the channel. This prevented the diffusion of fluorophore into the surrounding hydrogel and allowed prolonged imaging of the samples.

In experiments with the rotary UPC (Figure 8A), the GelMA bioink containing fluorescently labeled hASC and CM was supplemented with a UV absorptive dye (FD&C yellow^[58]) to allow photocrosslinking of each layer without excessive photocrosslinking of the layer underneath. Herein, dye added at a concentration of 0.03% w/v^[58] along with 0.25% w/v of LAP photoinitiator provided a consistent a curing depth of 1.5 mm (derived from pilot experiments). After deposition of 4 ml of GelMA bioink for the first layer, the transducers were actuated for 90 s to allow the cells to pattern, followed by photocrosslinking using an overhead laser diode^[37] (405 nm, Lights88) with a laser aperture diameter of 2 mm, attached to a modified extrusion printhead of a BioAssemblyBot (Advanced Solutions Life Sciences) at a speed of 2 mm/s to photocrosslink each layer. After crosslinking of the first layer, the second layer of 4 ml of GelMA was added followed by rotating the rotary fixture by 45° (with respect to the first layer) and photocrosslinking. For the third layer, the rotary fixture was rotated by another 45° (i.e., 90° with

respect to the first layer) followed by photocrosslinking. The excess bioink surrounding the

construct was removed, and the construct (4.5 mm thick) was imaged using a confocal microscope.

In the study to demonstrate the fabrication of a construct to mimic annulus fibrosus organization

(Figure 8B), hybrid GelMA containing CM and hASC was allowed to thermo-reversibly crosslink

at 10°C for 5 min while the transducer was actuated in burst mode similar to the previous studies

in the UPC with a circular reflector. The photocrosslinking protocol was the same as that used for

the previous study with the rotary UPC. The GelMA was heated to 37°C to remove any non-

photocrosslinked bioink.

Constructs in all these studies were imaged at room temperature using a confocal

microscope (Fluoview 3000, Olympus).

Statistical analysis: Statistical analysis was performed in JMP® (SAS, Cary, NC) at

significance level of $\alpha = 0.05$ using a one-way ANOVA (for studies corresponding to results shown

in Figures 2D and E) and two-way ANOVA (for studies corresponding to results shown in Figures

2C, 3C and 4B-E) with Tukey HSD post hoc tests. Sample size was kept constant at n = 3 for all

the studies.

Supporting Information

Supporting Information is available from the Wiley Online Library or from the author.

Acknowledgements

This work was supported by grants from the US National Science Foundation (NSF 1652489) and

US National Institutes of Health (NIH AR075261). The authors also thank Dr. Karl Schuchard, Dr.

Behnam Pourdeyhimi, and Mr. Bruce Anderson from North Carolina State University for creating

samples of melt blown PCL that served as the starting material for the polymer microfibers used in

this study.

Received: will be filled in by the editorial staff

Revised: will be filled in by the editorial staff

Published online: will be filled in by the editorial staff

References

- [1] J. Wong, E. Kuhl, Comput. Methods Biomech. Biomed. Engin. 2014, 17, 1217.
- [2] T. Arts, K. D. Costa, J. W. Covell, A. D. McCulloch, *Am. J. Physiol. Hear. Circ. Physiol.* 2001, 280, DOI 10.1152/ajpheart.2001.280.5.h2222.
- [3] A. Silvestri, M. Boffito, S. Sartori, G. Ciardelli, *Macromol. Biosci.* **2013**, *13*, 984.
- [4] P. Ferraiuoli, L. S. Fixsen, B. Kappler, R. G. P. Lopata, J. W. Fenner, A. J. Narracott, *Med. Eng. Phys.* **2019**, *74*, 146.
- [5] R. A. Neal, A. Jean, H. Park, P. B. Wu, J. Hsiao, G. C. Engelmayr, R. Langer, L. E. Freed, *Tissue Eng. Part A* **2013**, *19*, 793.
- [6] R. L. Mauck, B. M. Baker, N. L. Nerurkar, J. A. Burdick, W.-J. Li, R. S. Tuan, D. M. Elliott, *Tissue Eng. Part B Rev.* **2009**, *15*, 171.
- [7] C. A. D'Angelis, J. J. Coalson, R. M. Ryan, in *Pediatr. Crit. Care*, Elsevier Inc., **2011**, pp. 490–498.
- [8] J. Nasehi Tehrani, A. McEwan, J. Wang, Med. Phys. 2016, 43, 5493.
- [9] V. I. Egorov, I. V. Schastlivtsev, E. V. Prut, A. O. Baranov, R. A. Turusov, *J. Biomech.*2002, 35, 1417.
- [10] B. M. Whited, M. N. Rylander, Biotechnol. Bioeng. 2014, 111, 184.
- [11] R. A. Shirwaiker, M. B. Fisher, B. Anderson, K. G. Schuchard, P. B. Warren, B. Maze, P. Grondin, F. S. Ligler, B. Pourdeyhimi, *Tissue Eng. Part C Methods* **2020**, ten. TEC.2020.0098.
- [12] P. B. Warren, P. Huebner, J. T. Spang, R. A. Shirwaiker, M. B. Fisher, *Connect. Tissue Res.* **2017**, *58*, 342.
- [13] N. Noor, A. Shapira, R. Edri, I. Gal, L. Wertheim, T. Dvir, Adv. Sci. 2019, 6, 1900344.
- [14] M. A. Skylar-Scott, S. G. M. Uzel, L. L. Nam, J. H. Ahrens, R. L. Truby, S. Damaraju, J. A. Lewis, *Sci. Adv.* 2019, 5, eaaw2459.
- [15] Q. Mao, Y. Wang, Y. Li, S. Juengpanich, W. Li, M. Chen, J. Yin, J. Fu, X. Cai, *Mater. Sci. Eng. C* **2020**, *109*, 110625.

- [16] S. Knowlton, S. Tasoglu, Trends Biotechnol. 2016, 34, 681.
- [17] S. Michael, H. Sorg, C. T. Peck, L. Koch, A. Deiwick, B. Chichkov, P. M. Vogt, K. Reimers, *PLoS One* **2013**, *8*, e57741.
- [18] V. Lee, G. Singh, J. P. Trasatti, C. Bjornsson, X. Xu, T. N. Tran, S. S. Yoo, G. Dai, P. Karande, *Tissue Eng. Part C Methods* **2014**, *20*, 473.
- [19] K. Park, H.-J. Suk, D. Akin, R. Bashir, Lab Chip 2009, 9, 2224.
- [20] T. P. Hunt, R. M. Westervelt, Biomed. Microdevices 2006, 8, 227.
- [21] R. K. Pirlo, Z. Ma, A. Sweeney, H. Liu, J. X. Yun, X. Peng, X. Yuan, G. X. Guo, B. Z. Gao, Rev. Sci. Instrum. 2011, 82, 013708.
- [22] Z. Ma, Q. Liu, H. Liu, H. Yang, J. X. Yun, M. Xu, C. A. Eisenberg, T. K. Borg, R. Markwald, B. Z. Gao, *Cell. Mol. Bioeng.* 2012, 5, 327.
- [23] W. Liu, N. Dechev, I. G. Foulds, R. Burke, A. Parameswaran, E. J. Park, *Lab Chip* **2009**, 9, 2381.
- [24] T. Kimura, Y. Sato, F. Kimura, M. Iwasaka, S. Ueno, *Langmuir* **2005**, *21*, 830.
- [25] J. Shi, D. Ahmed, X. Mao, S.-C. S. Lin, A. Lawit, T. J. Huang, *Lab Chip* **2009**, *9*, 2890.
- [26] B. W. Drinkwater, *Lab Chip* **2016**, *16*, 2360.
- [27] S. Zhang, L. Yan, M. Altman, M. Lässle, H. Nugent, F. Frankel, D. A. Lauffenburger, G. M. Whitesides, A. Rich, *Biomaterials* 1999, 20, 1213.
- [28] C. A. Scotchford, C. P. Gilmore, E. Cooper, G. J. Leggett, S. Downes, *J. Biomed. Mater. Res.* **2002**, *59*, 84.
- [29] F. Guo, Z. Mao, Y. Chen, Z. Xie, J. P. Lata, P. Li, L. Ren, J. Liu, J. Yang, M. Dao, S. Suresh, T. J. Huang, *Proc. Natl. Acad. Sci. U. S. A.* 2016, 113, 1522.
- [30] H. K. Chu, Z. Huan, J. K. Mills, J. Yang, D. Sun, Lab Chip 2015, 15, 920.
- [31] J. P. K. Armstrong, J. L. Puetzer, A. Serio, A. G. Guex, M. Kapnisi, A. Breant, Y. Zong, V. Assal, S. C. Skaalure, O. King, T. Murty, C. Meinert, A. C. Franklin, P. G. Bassindale, M. K. Nichols, C. M. Terracciano, D. W. Hutmacher, B. W. Drinkwater, T. J. Klein, A. W.

- Perriman, M. M. Stevens, Adv. Mater. 2018, 30, DOI 10.1002/adma.201802649.
- [32] F. Gesellchen, A. L. Bernassau, T. Déjardin, D. R. S. Cumming, M. O. Riehle, *Lab Chip* **2014**, *14*, 2266.
- [33] B. Kang, J. Shin, H. J. Park, C. Rhyou, D. Kang, S. J. Lee, Y. sup Yoon, S. W. Cho, H. Lee, *Nat. Commun.* **2018**, *9*, 1.
- [34] D. Petta, V. Basoli, D. Pellicciotta, R. Tognato, J. Barcik, C. Arrigoni, E. Della Bella, A. R. Armiento, C. Candrian, R. G. Richards, M. Alini, M. Moretti, D. Eglin, T. Serra, *Biofabrication* 2020, 13, 015004.
- [35] P. Chansoria, L. K. Narayanan, K. Schuchard, R. A. Shirwaiker, *Biofabrication* **2019**, *11*, 14861.
- [36] P. Chansoria, R. Shirwaiker, Sci. Rep. 2019, 9, 13889.
- [37] P. Chansoria, R. Shirwaiker, *Addit. Manuf.* **2020**, *32*, 101042.
- [38] C. Bouyer, P. Chen, S. Güven, T. T. Demirtaş, T. J. F. Nieland, F. Padilla, U. Demirci, *Adv. Mater.* **2016**, *28*, 161.
- [39] P. Chen, S. Güven, O. B. Usta, M. L. Yarmush, U. Demirci, *Adv. Healthc. Mater.* **2015**, *4*, 1937.
- [40] K. A. Garvin, D. Dalecki, D. C. Hocking, Ultrasound Med. Biol. 2011, 37, 1853.
- [41] H. Aubin, J. W. Nichol, C. B. Hutson, H. Bae, A. L. Sieminski, D. M. Cropek, P. Akhyari, A. Khademhosseini, *Biomaterials* **2010**, *31*, 6941.
- [42] M. Rizwan, G. S. L. Peh, H. P. Ang, N. C. Lwin, K. Adnan, J. S. Mehta, W. S. Tan, E. K. F. Yim, *Biomaterials* 2017, 120, 139.
- [43] P. Chansoria, S. Asif, K. Polkoff, J. Chung, J. A. Piedrahita, R. A. Shirwaiker, *ACS Biomater. Sci. Eng.* **2021**, acsbiomaterials.1c00635.
- [44] K. Yue, G. Trujillo-de Santiago, M. M. Alvarez, A. Tamayol, N. Annabi, A. Khademhosseini, *Biomaterials* **2015**, *73*, 254.
- [45] D. Haydock, J. Phys. A. Math. Gen. 2005, 38, 3279.

- [46] S. Asif, P. Chansoria, R. Shirwaiker, J. Manuf. Process. 2020, 56, 1340.
- [47] F. P. W. Melchels, M. A. N. Domingos, T. J. Klein, J. Malda, P. J. Bartolo, D. W. Hutmacher, *Prog. Polym. Sci.* **2012**, *37*, 1079.
- [48] G. Chu, C. Shi, J. Lin, S. Wang, H. Wang, T. Liu, H. Yang, B. Li, Adv. Exp. Med. Biol. 2018, 1078, 409.
- [49] D. Eyre, Arthritis Res. Ther. 2001 41 **2001**, 4, 1.
- [50] J. M. Lee, W. Y. Yeong, J. R. Soc. Interface 2020, 17, DOI 10.1098/RSIF.2020.0294.
- [51] S. P. Pilipchuk, A. Monje, Y. Jiao, J. Hao, L. Kruger, C. L. Flanagan, S. J. Hollister, W. V Giannobile, S. P. Pilipchuk, C. L. Flanagan, S. J. Hollister, W. V Giannobile, A. Monje, Y. Jiao, J. Hao, L. Kruger, *Adv. Healthc. Mater.* **2016**, *5*, 676.
- [52] C. Imashiro, B. Kang, Y. Lee, Y.-H. Hwang, S. Im, D.-E. Kim, K. Takemura, H. Lee, *Microsystems Nanoeng. 2021 71* **2021**, 7, 1.
- [53] M. E. M. Stamp, M. S. Brugger, A. Wixforth, C. Westerhausen, *Biomater. Sci.* **2016**, *4*, 1092.
- [54] P. Chansoria, K. Schuchard, R. A. Shirwaiker, *WIREs Nanomedicine and Nanobiotechnology* **2020**, DOI 10.1002/wnan.1673.
- [55] M. Castilho, M. de Ruijter, S. Beirne, C. C. Villette, K. Ito, G. G. Wallace, J. Malda, *Trends Biotechnol.* **2020**, *38*, 1316.
- [56] T. Osaki, V. Sivathanu, R. D. Kamm, *Biomaterials* **2018**, *156*, 65.
- [57] P. Chansoria, E. L. Etter, J. Nguyen, *Trends Biotechnol.* 2021, DOI 10.1016/J.TIBTECH.2021.07.001.
- [58] B. Grigoryan, S. J. Paulsen, D. C. Corbett, D. W. Sazer, C. L. Fortin, A. J. Zaita, P. T. Greenfield, N. J. Calafat, J. P. Gounley, A. H. Ta, F. Johansson, A. Randles, J. E. Rosenkrantz, J. D. Louis-Rosenberg, P. A. Galie, K. R. Stevens, J. S. Miller, *Science* (80-.). 2019, 364, 458.
- [59] I. M. El-Sherbiny, M. H. Yacoub, Glob. Cardiol. Sci. Pract. 2013, 2013, 38.
- [60] P. Maturavongsadit, L. K. Narayanan, P. Chansoria, R. Shirwaiker, S. R. Benhabbour, ACS

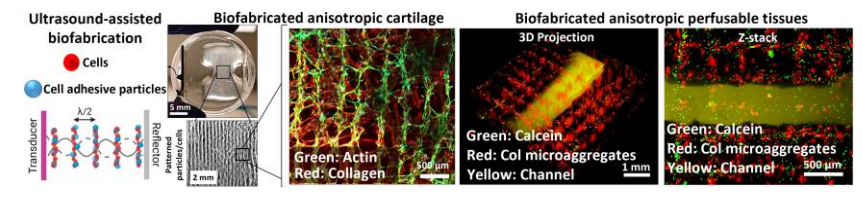
- Appl. Bio Mater. 2021, 4, 2342.
- [61] P. Chansoria, L. K. Narayanan, M. Wood, C. Alvarado, A. Lin, R. A. Shirwaiker, *ACS Biomater. Sci. Eng.* **2020**, *6*, 5191.
- [62] T. S. Jang, H. Do Jung, H. M. Pan, W. T. Han, S. Chen, J. Song, *Int. J. Bioprinting* 2018, 4, DOI 10.18063/IJB.v4i1.126.
- [63] A. Omidinia-Anarkoli, S. Boesveld, U. Tuvshindorj, J. C. Rose, T. Haraszti, L. De Laporte, *Small* **2017**, *13*, DOI 10.1002/smll.201702207.
- [64] Bush NL, Hill CR., Ultrasound Med. Biol. 1983.
- [65] M.-S. Scholz, B. W. Drinkwater, T. M. Llewellyn-Jones, R. S. Trask, *IEEE Trans. Ultrason. Ferroelectr. Freq. Control* **2015**, *62*, 1845.
- [66] J. Schindelin, I. Arganda-Carreras, E. Frise, V. Kaynig, M. Longair, T. Pietzsch, S. Preibisch, C. Rueden, S. Saalfeld, B. Schmid, J.-Y. Tinevez, D. J. White, V. Hartenstein, K. Eliceiri, P. Tomancak, A. Cardona, *Nat. Methods* 2012, 9, 676.

Table of Contents

A novel ultrasound-assisted biofabrication approach is used in conjunction with hybrid bioink formulations containing cells and cell-adhesion-promoting additives to fabricate anisotropic tissue constructs. The hybrid constructs featuring patterned cells and additives demonstrate enhanced mechanical strength and elongated cell and cell-secreted collagen morphology. The process is appropriately hybridized with extrusion printing and stereolithography to create constructs with complex anisotropy and perfusable channels.

P. Chansoria, S. Asif, N. Gupta, J. Piedrahita, R. A. Shirwaiker*

Multiscale Anisotropic Tissue Biofabrication via Bulk Acoustic Patterning of Cells and Functional Additives in Hybrid Bioinks



Supporting Information

Multiscale Anisotropic Tissue Biofabrication via Bulk Acoustic Patterning of Cells and Functional Additives in Hybrid Bioinks

Parth Chansoria, Suleman Asif, Nithin Gupta, Jorge Piedrahita, Rohan A. Shirwaiker*

Analytical model (theory) for the ultrasound-assisted patterning of cells and additives within hydrogel matrices

Here we explain the analytical model describing physics of the cell and additive alignment process, highlighting the forces acting on these particles to pattern them to nearest pressure nodes within the bioink. The values of all the variables used in the theoretical framework have been provided in **Table S1**. As shown in Figure 1A, when the piezoelectric transducer vibrates, it generates an acoustic wave in the medium, and interaction of the transmitted wave with reflected wave results in the formation of a standing bulk acoustic wave (SBAW) within the bioink^[1]. The pressure distribution p(x,t) in this standing wave field in the medium can be obtained by combining continuity and Euler's equations as

$$\frac{1}{c_g^2} \frac{\partial^2 p}{\partial t^2} - \left(\frac{\partial^2 p}{\partial x^2} \right) = 0 \tag{1}$$

where c_g = longitudinal speed of sound in the GelMA bioink. Considering the pressure fields produced from the transmitted and reflected waves, the solution to equation (1) can be defined as a combinatorial complex harmonic expression as

$$p(x,t) = P_{transducer} + P_{reflector}$$
 (2)

$$P_{transmitted} = Ae^{j(2\pi ft - kx)}$$
 (3)

$$P_{\text{reflected}} = Be^{j(2\pi ft + kx)} \tag{4}$$

where $P_{transmitted}$ = pressure field along positive x-axis, $P_{reflected}$ = pressure field along negative x-axis, A and B = complex constants, f = frequency of acoustic wavefield, and k = wave number. At the interface of the bioink contact with the transducer (x = 0), the pressure is given as

$$p(0,t) = P_0 e^{j(2\pi ft)}$$
 (5)

where P_0 = pressure amplitude.

A normal incidence of the planar wave leads to zero fluid velocity boundary condition at the reflector as

$$v(L,t) = -\frac{1}{\rho_a} \int_0^t \frac{\partial p}{\partial x} dt = 0$$
 (6)

where v = bioink velocity along x-axis, $\rho_g = mass$ density of GelMA, and L = distance between the transducer and reflector. The equation for the pressure distribution in SBAW is obtained by solving equations (2)-(6).

$$p(x,t) = P_0 \cos(2\pi f t) \cos(kx)$$
 (7)

The distance between the transducer and reflector needs to be integer multiple of half the wavelength given by constraint

$$L = \frac{n\lambda}{2} \tag{8}$$

where n = integer number of nodes within the standing wave in the medium, and λ = wavelength of the acoustic wavefield. The SBAW contains alternate node and antinode planes with a distance of $\lambda/4$ between them. At each antinode, SBAW generates a radiation force (F_{radiation}) on the particles to pattern them towards the closest nodes, resulting in arrays of particles along nodal planes

$$F_{\text{radiation}} = F_0 \sin(2kx) \tag{9}$$

where F_0 is defined as amplitude of the acoustic radiation force acting on the particles to align them towards pressure nodes. This amplitude is dependent on the shape of the particles, and is different for cells, CM, and PM. For the cells and CM, which are assumed to be spheres, the F_0 is defined as a function of the acoustic potential amplitude (U_0) and the acoustophoretic coefficient (Φ) as

$$F_0 = 2kU_0\Phi \tag{10}$$

where
$$U_0 = \frac{P_0^2 V}{8\rho_g c_g^2}$$
 (11)

and
$$\Phi = \frac{5\gamma - 2}{2\gamma + 1} - \frac{1}{\gamma\beta^2}$$
 (12)

where V = volume of cell/CM, γ = ratio of the densities of the cell or CM to that of GelMA = ρ_c/ρ_g , and β = ratio of speed of sound in a cell or CM to that in GelMA= c_c/c_g .

For the PM, which are modeled as cylinders, and the $F_{radiation}$ acting on the cylinder in a standing wave acoustic field is calculated based on a previous study^[2] as the sum of the contributions from the time average potential energy $\langle P_{\phi} \rangle$, kinetic energy $\langle P_{q} \rangle$, and a contribution due to the motion of the PM $\langle P_{r} \rangle$

$$F_{\text{radiation}} = \langle P_{\phi} \rangle + \langle P_{q} \rangle + \langle P_{\zeta} \rangle \tag{13}$$

The contribution of $F_{radiation}$ on cylinder due to the time-averaged potential energy can be calculated as

$$\langle P_{\phi} \rangle = -\frac{\pi a \rho_{g} (V_{0}' \omega)^{2}}{4 c_{g}^{2}} \operatorname{Re}[f_{1}(kr)]$$
(14)

where

$$\begin{split} f_{1}(ka) &= \left(2AB + \frac{3}{2}BC\right) + \frac{BE}{2} \frac{H_{0}^{(1)}(ka)}{H_{0}^{(1)'}(ka)} \\ &+ \left(A + \frac{3}{4}C\right) \left(D + \frac{3}{4}F + \frac{v_{x}}{v_{0}'k}\right) \frac{H_{1}^{(1)}(ka)}{H_{1}^{(1)'}(ka)} + \frac{BE}{4} \frac{H_{2}^{(1)}(ka)}{H_{2}^{(1)'}(ka)} \\ &+ \frac{BE}{2} \frac{H_{0}^{(2)}(ka)}{H_{0}^{(2)'}(ka)} + \frac{E}{2} \left(D + \frac{3}{4}F + \frac{v_{x}}{v_{0}'k}\right) \frac{H_{0}^{(2)}(ka)H_{1}^{(1)}(ka)}{H_{0}^{(2)'}(ka)H_{1}^{(1)'}(ka)} \\ &+ \left(D + \frac{3}{4}F + \frac{v_{x}}{v_{0}'k}\right) \left(A + \frac{3}{4}C\right) \frac{H_{1}^{(2)}(ka)}{H_{1}^{(2)'}(ka)} \\ &+ \frac{E}{2} \left(D + \frac{3}{4}F + \frac{v_{x}}{v_{0}'k}\right) \frac{H_{1}^{(2)}(ka)H_{0}^{(1)}(ka)}{H_{1}^{(2)'}(ka)H_{0}^{(1)'}(ka)} \\ &+ \frac{E}{4} \left(D + \frac{3}{4}F + \frac{v_{x}}{v_{0}'k}\right) \frac{H_{1}^{(2)}(ka)H_{2}^{(1)}(ka)}{H_{1}^{(2)'}(ka)H_{1}^{(1)'}(ka)} \\ &+ \frac{E}{4} \left(D + \frac{3}{4}F + \frac{v_{x}}{v_{0}'k}\right) \frac{H_{1}^{(2)}(ka)H_{1}^{(1)'}(ka)}{H_{2}^{(2)'}(ka)H_{1}^{(1)'}(ka)} \\ &+ \frac{E}{4} \left(D + \frac{3}{4}F + \frac{v_{x}}{v_{0}'k}\right) \frac{H_{2}^{(2)}(ka)H_{1}^{(1)'}(ka)}{H_{2}^{(2)'}(ka)H_{1}^{(1)'}(ka)} \end{split}$$

Here, A, B, C, D, E and F are constants that are described from the boundary conditions on the surface of the cylinder.

$$A = 1 - \frac{(kh)^2}{2!} + \frac{(kh)^4}{4!} - \frac{(kh)^6}{6!} + \frac{(kh)^8}{8!}$$
 (16)

$$B = -(kh)(ka) + \frac{(kh)^3(ka)}{3!} - \frac{(kh)^5(ka)}{5!} - \frac{(kh)^7(ka)}{7!}$$
(17)

$$C = -\frac{(ka)^2}{2!} + \frac{6(kh)^2(ka)^2}{4!} - \frac{15(kh)^4(ka)^2}{6!} + \frac{28(kh)^6(ka)^2}{8!}$$
(18)

$$D = kh - \frac{(kh)^3}{3!} + \frac{(kh)^5}{5!} - \frac{(kh)^7}{7!}$$
(19)

$$E = ka - \frac{(kh)^{2}(ka)}{2!} + \frac{(kh)^{4}(ka)}{4!} - \frac{(kh)^{6}(ka)}{6!}$$
(20)

$$F = -\frac{(kh)(ka)^2}{2!} + \frac{2(kh)^3(ka)^2}{4!} - \frac{23(kh)^5(ka)^2}{6!}$$
 (21)

Along x-direction, the particle velocity of the PM (cylinder) is given by

$$v_{x} = V_{0}^{'} \frac{B + \left(D + \frac{3F}{4}\right) \frac{H_{1}^{(2)}}{H_{1}^{(2)}(ka)}}{\frac{\rho_{c}}{\rho_{g}} \frac{1}{k_{1}^{(2)}(ka)} \frac{H_{1}^{(2)}(ka)}{H_{1}^{(2)}(ka)}}$$
(22)

where $V_0' = \frac{V_0}{k}$ where V_0 is the velocity amplitude at the source, and $H_n^{(1)}$ (ka) and $H_n^{(2)}$ (ka) are nth-order Hankel functions of the first and second kind respectively such that

$$H_n^{(2)'}(kr) = \partial_{kr} H_n^{(2)}(kr)$$
 (23)

The acoustic intensity is related to the pressure as

$$I = \frac{P^2}{2\rho_g c_g} \tag{24}$$

The contribution of F_{radiation} due to the time-averaged kinetic energy is obtained as

$$\langle P_{\rm q} \rangle = \frac{\rho_{\rm g} \pi V_0'}{8a} \operatorname{Re} f_3(kr)$$
 (25)

where

$$\begin{split} f_3(kr) &= C \left(D + \frac{3}{4} F + \frac{v_x}{V_0' k} \right) \left[\frac{H_1^{(2)}(ka)}{H_1^{(2)'}(ka)} + \frac{H_1^{(1)}(ka)}{H_1^{(1)'}(ka)} \right] + 2BC - CG \\ &+ \left[\left(D + \frac{3}{4} F + \frac{v_x}{V_0' k} \right) \frac{H_1^{(2)}(ka)}{H_1^{(2)'}(ka)} + B - \frac{G}{2} \right] \frac{EH_2^{(1)}(ka)}{H_2^{(1)'}(ka)} \\ &+ \left[\left(D + \frac{3}{4} F + \frac{v_x}{V_0' k} \right) \frac{H_1^{(1)}(ka)}{H_1^{(1)'}(ka)} + B - \frac{G}{2} \right] \frac{EH_2^{(2)}(ka)}{H_2^{(2)'}(ka)} \end{split}$$

(26)

The contribution due to motion of the cylinder is given as

$$P_{\zeta} = -\frac{\rho_g \pi}{2} \text{Re} \left[v_x \left(C + E \frac{H_2^{(1)}(ka)}{H_2^{(1)'}(ka)} \right) \right]$$
 (27)

The F_0 can be calculated by substituting $h = (2n+1)\lambda/8$ in equations (16)-(21) for constants A to F. This value of h corresponds to locations between nodes and antinodes where $F_{radiation}$ is maximum.

For the cells and additives traveling from or near the antinodes to the nodal regions, the equation of motion is provided as a non-linear ordinary differential equation combining the $F_{radiation}$ and the drag force (F_{drag}) as

$$m\ddot{x} + F_{\text{radiation}} + F_{\text{drag}} = 0 \tag{28}$$

where \ddot{x} = instantaneous acceleration of the particles. To determine the expression for the drag forces on the PM, the PM are considered spheres. This is because the orientation of cylindrical PMs is not known and will be highly variable during motion from antinodes to nodes. Therefore, collectively, the F_{drag} acting on cells, CM and PM can be given as

$$F_{drag} = 6\pi \eta r \dot{x} \tag{29}$$

where η = dynamic viscosity of the bioink, r = radius of the particles, and \dot{x} is the instantaneous velocity of the particles. Assuming the particle is travelling at a constant speed (\ddot{x} = 0), the analytical solution for equation (28) to obtain instantaneous position (x(t)) of a particle moving from antinodal position x_0 to the node is given as

$$x(t) = \frac{1}{k} \tan^{-1} \left(\tan(kx_0) e^{\frac{-2F_0 t}{3\lambda \eta r}} \right)$$
 (30)

Using this equation, time taken by particle to travel from its initial position x_0 to final position x_f is given as

$$t_{\text{align_continuous}} = \frac{3\lambda \eta r}{2F_0} \ln \left(\frac{\tan(kx_0)}{\tan(kx_f)} \right)$$
 (31)

This is the time to align is when the transducers are actuated continuously. However, in the present work, to prevent overheating of the transducers and to maintain cell viability, the transducers are actuated for 1 s, followed by 1 s pause^[1]. Hence, the time to align in burst mode is assumed to be twice that in the continuous mode.

$$t_{align_burst} = 2t_{align_continuous}$$
 (32)

Table S1. The values of all the variables used in the theoretical framework described above. These values and their corresponding implementation in the analytical expressions described in the theory are used to derive the expressions of the movements of the cells and additives as shown in Figure 3A.

Variable	Units	Value
Ultrasound frequency	MHz	2
Acoustic pressure amplitude	KPa	400
Viscosity of GelMA	cР	70
Mass density of GelMA	kg/m ³	1020
Mass density of cells	kg/m ³	1050
Mass density of CM	kg/m ³	1300
Mass density of PM	kg/ m ³	1145
Speed of sound in GelMA	m/s	1534
Speed of sound in cells	m/s	1530
Speed of sound in CM	m/s	1540
Speed of sound in PM	m/s	1150
Diameter of cells	μm	24
Diameter of CM	μm	11.2
Diameter of PM	μm	6.2
Length of PM	μm	52.3

Supporting Information References

- [1] P. Chansoria, R. Shirwaiker, Sci. Rep. 2019, 9, 13889.
- [2] D. Haydock, J. Phys. A. Math. Gen. 2005, 38, 3279.